Engineering Structures 213 (2020) 110575

Contents lists available at ScienceDirect

Engineering Structures

journal homepage: www.elsevier.com/locate/engstruct

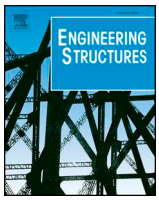

Buffeting response of long-span bridges considering uncertain turbulence parameters using the environmental contour method

Tor M. Lystad[a,b,*], Aksel Fenerci[b], Ole Øiseth[b]

[a] Bridge Department, Norconsult AS, Sandvika, Norway
[b] Department of Structural Engineering, Norwegian University of Science and Technology, Trondheim, Norway

ARTICLE INFO

Keywords:
Long-span bridge
Environmental contour method
Turbulence variability
Probabilistic design

ABSTRACT

Full-scale monitoring of the Hardanger Bridge has revealed significant turbulence-induced variability in the measured acceleration response. In this paper, a probabilistic model is used to describe the uncertain turbulence parameters, and the environmental contour method is used to investigate the long-term root-mean-square (RMS) response of the Hardanger Bridge. The results show that turbulence-induced variability has a significant impact on the bridge girder section moments. It is also interesting that the critical combination of environmental parameters does not necessarily involve the maximum mean wind velocity. By using the environmental contour method to account for turbulence uncertainty, the scattered acceleration RMS response measurements from the Hardanger Bridge are successfully eclipsed by 100-year return period response estimates, showing vast improvements compared with the traditional design methodology. The investigations presented in this paper show that the environmental contour method can be used to improve the accuracy and reduce the uncertainty in buffeting response calculations for long-span bridge design.

1. Introduction

The trend in international bridge engineering is that increasingly longer passages are crossed with long-span bridges. As experience and development progress, more audacious bridge crossings are considered, such as the Messina Strait and the Strait of Gibraltar. In Norway, the government is planning to build a continuous highway along the west coast of the country [1]. Such a highway would have to cross several fjords with extreme long-span bridges, replacing the current ferry connections. Many of the bridge concepts under consideration are extremely slender, such as floating bridges spanning up to 5500 m and suspension bridges with main spans over 3000 m. Buffeting response from turbulent wind loading governs the design stresses for these types of structures, so uncertainties connected to the description of the turbulent wind field must be properly handled as it significantly affects the overall structural reliability.

Since 2013, the Norwegian University of Science and Technology has performed full-scale measurements of the wind field characteristics and acceleration responses of the Hardanger Bridge, the longest suspension bridge in Norway. The results from the measurement campaign have been presented in a series of papers [2–7], showing significant turbulence-induced variability in the measured dynamic response. Several full-scale measurement studies have been performed on long-span bridges around the world, showing similar variability in the measured response [8–17]. In the traditional design methodology for long-span bridges, only the mean wind velocity is treated as a stochastic variable because it is considered a very dominating load parameter. The corresponding turbulence parameters are then chosen deterministically based on design codes or site measurements. The results from the previously referenced studies indicate that this methodology is too simplified and may introduce significant uncertainty to the response estimates.

Long-term extreme response calculations have long been the standard for the design of offshore structures subjected to wave loading [18]. In such calculations, the load parameters and the short-term extreme response can be treated as stochastic variables. The environmental contour method [19] is an efficient approach to estimate the long-term extreme response by a short-term extreme value analysis. This method decouples the variability in the environmental parameters and the variability in the extreme response itself [20], and only the variability in the load parameters are considered directly. The effect of the extreme value uncertainty is often simplified by choosing a higher percentile of the short-term extreme response probability distribution as the design value. Environmental contours can be established using several methods, such as the inverse first order reliability method (FORM), inverse second order reliability method (SORM), the highest

* Corresponding author at:Bridge Department, Norconsult AS, Sandvika, Norway.
E-mail address: tor.m.lystad@ntnu.no (T.M. Lystad).

https://doi.org/10.1016/j.engstruct.2020.110575
Received 14 November 2019; Received in revised form 20 March 2020; Accepted 24 March 2020
Available online 10 April 2020

density contour method (HDC) or Monte Carlo simulation [21–23]. The inverse FORM is the most common and is the methodology applied in this work.

The environmental contour method can also be used to estimate the long-term response of structures subjected to wind loading with uncertain turbulence parameters [24–27]. Some studies using long-term response analyses for bridges, including the mean wind velocity distribution, have been performed [28,29], but long-term methods, including uncertain turbulence parameters, have not been studied in depth in the field of bridge engineering. Other probabilistic frameworks for buffeting response have also been suggested in the literature [30–37], but in long-term analyses, the probabilistic considerations are isolated to the dynamic extreme response, making it very interesting for practical design purposes. Probabilistic approaches, such as the environmental contour method, rely on a solid statistical description of the environmental variables, and some probabilistic models for uncertain turbulence parameters can be found in the literature [5,38].

The environmental load situations critical for design purposes are often the high return period cases. This means that the joint probability density functions (PDFs) for the environmental parameters need to describe the tail region properly or significant uncertainty can be expected [39]. Many efforts have been made to improve the environmental contour estimates for high return periods [40–45], but most studies focus on wave loading and not turbulent wind. In bridge engineering, the mean wind velocities with long return periods are often estimated from the extreme value distribution directly. In this paper, the tail of the mean wind velocity parent PDF is estimated from extreme wind measurements using asymptotic extreme value theory [46]. Instead of extrapolating the interesting tail region by fitting the PDF to the full mean wind velocity dataset, the less important low wind speed range is extrapolated based on the extreme values in the tail.

In Section 3 of this paper, environmental contours are established based on the probabilistic turbulence model for the Hardanger Bridge site developed by Fenerci and Øiseth [5]. In Section 4, the turbulence variability effect on the design response of the Hardanger Bridge girder has been investigated using constrained numerical optimization to identify the environmental situation most critical for the bridge girder section moments. The findings show that the design storm does not correspond to the event of the maximum mean wind velocity, but indeed, the turbulence parameters should be treated as stochastic variables. In Section 5, vast improvements are achieved by using this method to compare the calculated acceleration root-mean-square (RMS) response with the scattered response from the full-scale measurements of the Hardanger Bridge. The traditional approach is not able to describe the variability in the measured response, whereas the environmental contour method can be used to find an upper and lower bound for the response as a function of the mean wind velocity, corresponding well with the scattered response observed from the full-scale measurements.

The environmental contour method is suitable for design purposes, and the investigations presented in this paper show that it can be used for turbulent wind loads to improve the accuracy and reduce the uncertainty in buffeting response calculations for long-span bridges.

2. The environmental contour method

The environmental contour method can be used to identify design storms corresponding to a target statistical return period. Then, the critical combination of the environmental parameters on the contour for an interesting structural response can be identified. The environmental contours are based on the joint PDFs of two or more random variables. The inverse FORM technique requires taking combinations of stochastic variables in the standard normal space and transforming the variables into real space using linear-, Rosenblatt- or Nataf transformations [47]. As an example, a two-dimensional transformation is shown in Fig. 1, including the mean wind velocity and the along-wind turbulence standard deviation for the easterly winds.

In the standard normal space, the statistical return period for a short-term process is related to the reliability index, β, as follows:

$$\beta = -\Phi^{-1}(1/[\frac{R_{yr} \times 365.25 \times 24 \times 60}{T_s}]) \tag{1}$$

where Φ is the standard normal cumulative density function (CDF), R_{yr} is the statistical return period in years, and T_s is the short-term duration in minutes. Given the standard normal variables, $u_1, u_2, \dots, u_n$ and the related real stochastic variables, $v_1, v_2, \dots, v_n$, the following transformation into the real space is needed:

$$\Phi(u_1, u_2, \dots, u_n) \rightarrow F_{V_1 V_2 \dots V_n}(v_1, v_2, \dots, v_n) \tag{2}$$

where $F_{V_1 V_2 \dots V_n}(v_1, v_2, \dots, v_n)$ is the cumulative joint distribution of the real stochastic variables. If the real variables are uncorrelated, the variables can be transformed independently as follows:

$$F_{V_n}(v_n) = \Phi(u_n) \Leftrightarrow v_n = F_{V_n}^{-1}[\Phi(u_n)] \tag{3}$$

However, if the variables are correlated, the transformation becomes more complicated, and generally, a transformation procedure such as the Rosenblatt or Nataf transformation needs to be applied.

The Rosenblatt procedure [48] is a widely used transformation because it is general and quite simple to use. The transformation procedure is based on the relationship where the joint CDF can be established from the product of conditional marginal CDFs, as shown in Eq. (4):

$$\begin{aligned} &F_{V_1, V_2, \dots, V_{n-1}}(v_1, v_2, \dots, v_{n-1}) \\ &\quad = F_{V_1}(v_1) F_{V_2|V_1}(v_2|v_1) \dots F_{V_n|V_1, V_2, \dots, V_{n-1}}(v_n|v_1, v_2, \dots, v_{n-1}) \end{aligned} \tag{4}$$

The Rosenblatt procedure is a stepwise transformation using conditional CDFs as follows:

$$\begin{aligned} &F_{V_1}(v_1) = \Phi(u_1) \;\Leftrightarrow\; v_1 = F_{V_1}^{-1}[\Phi(u_1)] \\ &F_{V_2|V_1}(v_2|\, v_1) = \Phi(u_2) \;\Leftrightarrow\; v_2|\, v_1 = F_{V_2|V_1}^{-1}[\Phi(u_2)] \\ &F_{V_3|V_1, V_2}(v_3|\, v_1, v_2) = \Phi(u_3) \;\Leftrightarrow\; v_3|\, v_1, v_2 = F_{V_3|V_1, V_2}^{-1}[\Phi(u_3)] \\ &\qquad \dots \\ &F_{V_n|V_1, V_2, \dots, V_{n-1}}(v_n|\, v_1, v_2, \dots, v_{n-1}) = \Phi(u_n) \;\Leftrightarrow\; v_n|\, v_1, v_2, \dots, v_{n-1} \\ &\qquad\qquad = F_{V_n|V_1, V_2, \dots, V_{n-1}}^{-1}[\Phi(u_n)] \end{aligned} \tag{5}$$

In the special case where the stochastic variables are normally distributed in the real space, the transformation from the uncorrelated standard normal space to the correlated real space is linear. It can be shown that if $\mathbf{X}$ is a vector containing the real variables v_i and $\mathbf{Y}$ is a vector containing the standard normal uncorrelated variables u_i, then the transformation can be described as follows:

$$\boldsymbol{Y} = \boldsymbol{A}(\boldsymbol{X} - \boldsymbol{M}_X) \;\Leftrightarrow\; \boldsymbol{X} = \boldsymbol{A}^{-1}\boldsymbol{Y} + \boldsymbol{M}_X \tag{6}$$

where $\boldsymbol{M}_X = [\mu_{V_1} \;\; \mu_{V_2} \;\; \cdots \;\; \mu_{V_n}]^T$ is a vector containing the mean values of the normally distributed variables v_i, and $\mathbf{A}$ is a transformation matrix. For normally distributed variables, $\mathbf{A}$ can be calculated based on the covariance matrix $\mathbf{C}_{XX}$ as follows:

$$\boldsymbol{C}_{XX} = \begin{bmatrix} \sigma_{V_1}^2 & \rho_{12}\sigma_{V_1}\sigma_{V_2} & \cdots & \rho_{1n}\sigma_{V_1}\sigma_{V_n} \\ \rho_{21}\sigma_{V_2}\sigma_{V_1} & \sigma_{V_2}^2 & \cdots & \rho_{2n}\sigma_{V_2}\sigma_{V_n} \\ \cdots & \cdots & \cdots & \cdots \\ \rho_{n1}\sigma_{V_n}\sigma_{V_1} & \rho_{n2}\sigma_{V_n}\sigma_{V_2} & \cdots & \sigma_{V_n}^2 \end{bmatrix} \tag{7}$$

$$\begin{aligned} \boldsymbol{A} &= \boldsymbol{D}^T\boldsymbol{S}^T \\ \boldsymbol{D} &= diag\,[1/\sqrt{\lambda_j}\,],\; j = 1, 2, \dots, n \\ \boldsymbol{S} &= [\boldsymbol{S}_1 \;\; \boldsymbol{S}_2 \;\; \dots \;\; \boldsymbol{S}_n] \end{aligned} \tag{8}$$

where σ_{Vj} is the standard deviation, ρ_{jk} is the correlation coefficient between the normally distributed variables, λ_j is the eigenvalues and $\mathbf{S}_j$ is the eigenvector of the correlation matrix $\mathbf{C}_{XX}$. This transformation procedure is often referred to as the Singular Value Decomposition (SVD), but the transformation matrix $\mathbf{A}$ could also be found by Cholesky decomposition of $\mathbf{C}_{XX}$, which is Hermitian and positive definite:

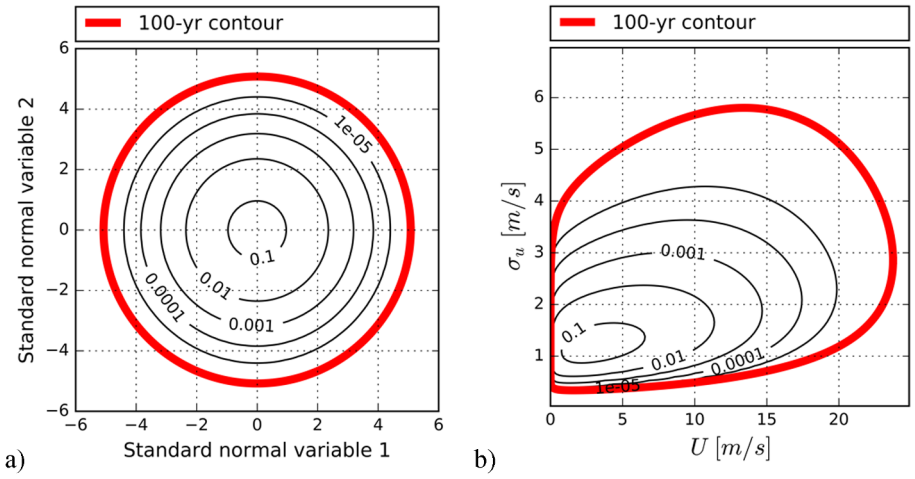

Fig. 1. Isoprobabilistic contours and the 100-year return period contour from the joint PDF of the mean wind velocity and the along-wind turbulence standard deviation for the easterly winds shown in a) the standard normal space, and b) the real space.

$$\boldsymbol{C}_{XX} = \boldsymbol{A}^{-1}\boldsymbol{A}^{-T} \tag{9}$$

If the stochastic variables are lognormally distributed in real space, the same transformation applies to find the associated normal distribution, and the lognormally distributed variables can be found as follows:

$$\boldsymbol{X} = \exp(\boldsymbol{A}^{-1}\boldsymbol{Y} + \boldsymbol{M}_X) \tag{10}$$

3. Wind field environmental contours for the Hardanger Bridge site

3.1. Probabilistic turbulence field

A probabilistic turbulence model using lognormal random turbulence parameters was established by Fenerci and Øiseth [5] for the Hardanger Bridge site in Norway (see Fig. 2), based on information from the full-scale measurement program thoroughly described in [2]. The turbulence spectra were assumed to be properly modeled using a Kaimal-type auto-spectra [49] and a normalized cross-spectra [50] as defined by Eq. (11). The cross-spectral densities between turbulence components, u and w are not described by the probabilistic model, and has been neglected in this study.

$$\frac{S_{u,w}f}{\sigma_{u,w}^2} = \frac{A_{u,w}f_z}{(1+1.5A_{u,w}f_z)^{5/3}},\ f_z = \frac{fz}{U}$$
$$C_{u,w} = \exp(-K_{u,w}\frac{f\Delta x}{U}) \tag{11}$$

where f is the frequency, z is the height above the ground, U is the mean wind velocity, $\sigma_{u,w}$ are the standard deviations of the turbulent process, $A_{u,w}$ are the nondimensional spectral parameters, and $K_{u,w}$ are the decay coefficients. The probabilistic model only considers along-span turbulence correlation, so the decay coefficients noted $K_{u,w}$ will refer to the along-span correlation throughout this paper. Using the definition in Eq. (11), the along-span turbulence cross-spectral density can be completely defined through six turbulence parameters for a given mean wind velocity and wind direction. Only two distinct wind directions, namely, the east and the west, were considered due to the channeled flow in the fjord, bounded by mountains on the sides (see Fig. 3). When the turbulence parameters are described with lognormal distributions, the full probabilistic model can be described by the distribution parameters and the correlation matrix given in Tables 1 and 2. The lognormal probability density function can be written as follows:

$$f(x) = \frac{1}{x\sigma\sqrt{2\pi}}\exp\left\{\frac{-(\ln x-\mu)^2}{2\sigma^2}\right\};\ x>0 \tag{12}$$

where μ (the mean of the natural logarithm of the random variable) and σ (the standard deviation of the natural logarithm of the random variable) are the distribution parameters, and x is the random variable.

For comparison, the turbulence parameters used in the design of the bridge are presented in Table 3. It should also be noted that all turbulence parameters shown in Tables 1–3 refer to the characteristics at the girder height, $z \approx 68$ m. Therefore, in all calculations presented in this paper, a constant vertical profile for both the turbulence and the mean wind velocity is assumed. This introduces a slight underestimation of the main cable load, however, the most influential contribution from the wind on the main cables is due to loading toward the midspan where the error from this simplification becomes small. Consequently, this simplification is not expected to affect the results or conclusions from this work.

3.2. PDF of the mean wind velocity

Since the probabilistic turbulence model described in the previous section is established conditional on the mean wind velocity, the PDF of the mean wind speed is also needed in estimating the environmental contours. However, the Hardanger Bridge full-scale measurement

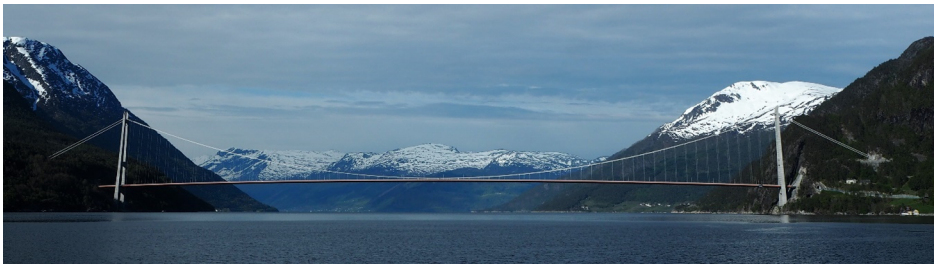

Fig. 2. The Hardanger Bridge seen from the east (Picture by the authors).

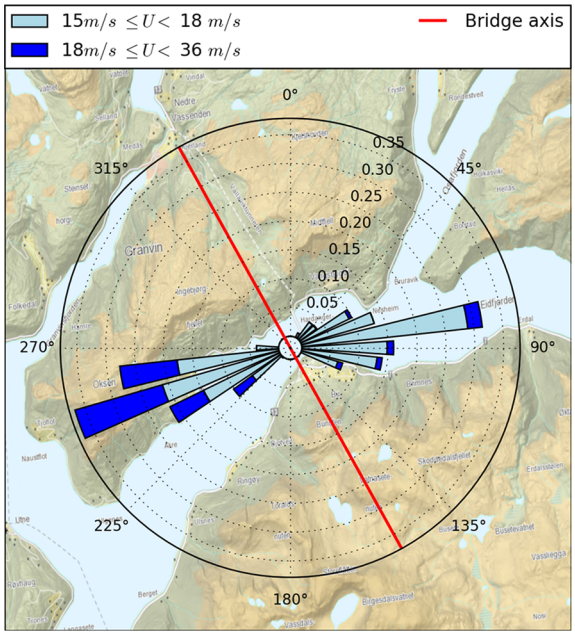

Fig. 3. Mean wind velocity wind rose at the Hardanger Bridge midspan. Only strong winds above 15 m/s are shown, and the rose shows wind speed percentages normalized for each wind direction summarizing to 100% for both easterly and westerly winds.

system was set up with a triggering setting that records only strong wind events. If a 1-minute mean wind velocity above 15 m/s is measured at any position along the bridge girder, the next 30 min is stored, including the first triggering minute. A histogram of all recorded 10-minute mean wind velocities is shown in Fig. 4. Because of the triggering system, the statistical basis is only complete for the high mean wind velocities. However, some data are available for lower wind speeds also, due to manually triggered periods of continuous measurements.

It is expected that the critical environmental parameter combinations for the buffeting response of the Hardanger Bridge are in the tail region of the mean wind velocity marginal PDF since this is the most influential parameter for this response [2]. Benefiting from this limited range of interest, the environmental contour in this region can be established directly based on the mean wind velocity extreme value distribution.

Lystad et al. [6] established the extreme value distributions for the measured mean wind velocity in 8 positions along the Hardanger Bridge span. The tail of the parent CDF can be transformed from an estimated extreme value distribution using asymptotic extreme value theory [46] as follows:

$$F_Z(x) = [F_X(x)]^N \Leftrightarrow F_X(x) = [F_Z(x)]^{1/N} \tag{13}$$

where $F_Z(x)$ is the annual extreme value CDF, $F_X(x)$ is the parent CDF and N is the number of annual 10-minute short-term periods. By using this relationship, the tail region of the mean wind velocity parent CDF can be described directly by the extreme value distribution.

The full dataset of the mean wind velocity is expected to follow a Weibull distribution, and the extremes will consequently follow a Gumbel distribution. In Fig. 5, the tail of the mean wind velocity parent CDF is shown for both the easterly and the westerly winds. The extreme value distribution was established using the method of independent storms (MIS) and the Gumbel-Lieblein BLUE method [52–54] based on the measured 16 strongest statistically independent storms (blue dots), from 4-years of continuous measurements. Details on the selection of independent storms and the extreme value distribution estimates can be found in [6]. As shown in Fig. 5, the transformed extreme value distribution (red line) is only able to describe the tail region of the parent distribution. To describe the full CDF for the mean wind velocity, the tail of the CDF is fitted to the transformed extreme value distribution using the least-squares technique. In this way, the body of the parent

Table 2
Correlation coefficient matrix from the probabilistic turbulence model, conditional on the wind direction [5].

		σ_u	σ_w	A_u	A_w	K_u	K_w
East	σ_u	1	0.7608	0.2641	0	0	0
	σ_w	0.7608	1	0	0.2571	0	0
	A_u	0.2641		1	0.1633	0	0
	A_w	0	0.2571	0.1633	1	0	0
	K_u	0	0	0	0	1	0.3261
	K_w	0	0	0	0	0.3261	1
West	σ_u	1	0.8148	0.4087	0	0	0
	σ_w	0.8148	1	0	0.2851	0	0
	A_u	0.4087	0	1	0.3065	0	0
	A_w	0	0.2851	0.3065	1	0	0
	K_u	0	0	0	0	1	0.4725
	K_w	0	0	0	0	0.4725	1

Table 3
Design basis turbulence characteristics in the girder height for the Hardanger Bridge [51].

	I_u	I_w	A_u	A_w	K_u	K_w
Design Basis	0.136	0.068	40.8	3.3	8.8	6.3

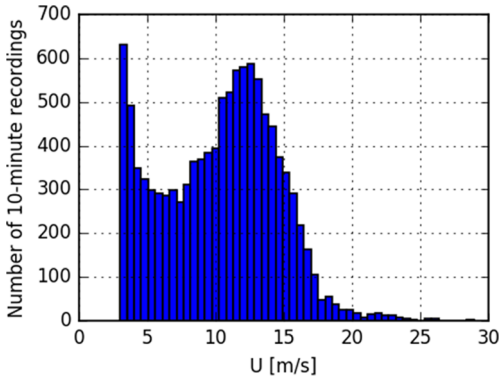

Fig. 4. Histogram of 10-minute midspan mean wind velocity recordings with 1 m/s sample bins.

Table 1
Lognormal distribution parameters from the probabilistic turbulence model, conditional on the mean wind velocity and wind direction [5].

		σ_u	σ_w	A_u	A_w	K_u	K_w
East	μ	0.122 + 0.039U	−0.657 + 0.032U	2.67 + 0.0248U	0.7076	1.9385	1.7932
	σ	0.2566	0.2632	0.4538	0.4466	0.2652	0.3423
West	μ	0.122 + 0.039U	−0.657 + 0.032U	2.407 + 0.048U	1.2075	2.1093	2.1633
	σ	0.3159	0.3021	0.5282	0.4943	0.268	0.3322

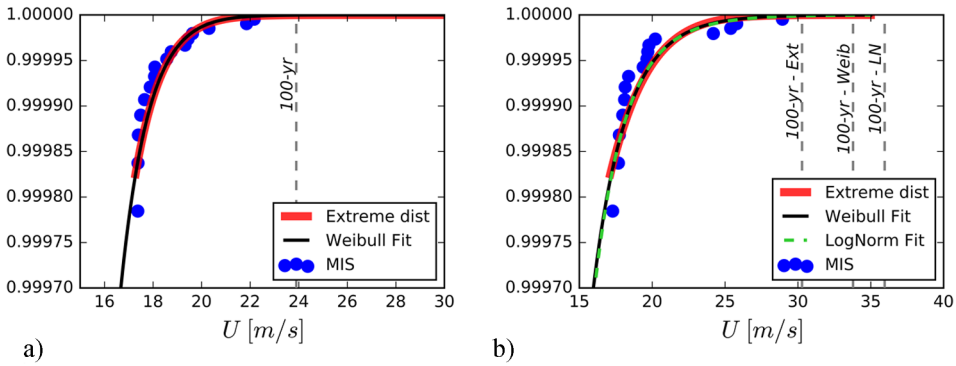

Fig. 5. Upper tail of the mean wind velocity parent CDF showing measured storms, the transformed extreme value distribution, and the fitted Weibull and lognormal distribution for (a) easterly winds and (b) westerly winds.

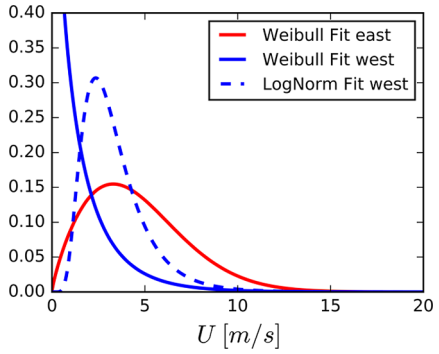

Fig. 6. Fitted parent PDFs for the mean wind velocity.

distribution is extrapolated from the important tail region instead of the other way around.

In Fig. 6, the fitted Weibull PDFs are shown in the full mean wind velocity range for both wind directions. The Weibull probability density function can be written as follows:

$$f(x) = \frac{k}{\lambda}\left(\frac{x}{\lambda}\right)^{(k-1)} \exp\left\{-\left(\frac{x}{\lambda}\right)^{k}\right\} ; x > 0 \tag{14}$$

where k and λ are the distribution parameters, and x is the random variable. The fitted Weibull distribution displays a classical shape for the easterly winds but not for the westerly winds. A lognormal distribution will also have Gumbel distributed extremes, so a lognormal CDF was also fitted to the data, displaying a more physical shape.

For the easterly winds, the fitted parent distribution follows the transformed extreme value distribution very well, estimating almost exactly the same 100-year return period mean wind velocity. However, for the westerly winds, both fitted parent distribution models differ slightly from the transformed extreme value distribution, resulting in relatively large deviations in the 100-year return period estimates (see Table 5). The fitted distribution parameters are shown together with the R-squared values in Table 4. The R-squared values are quite close to 1 for all the models, but still the deviation in high return period estimates becomes large, illustrating the sensitivity of these estimates.

It should be noted that Eq. (13) assumes independence between the drawn values form the random variable, X. When predicting the extreme value distribution $F_Z(x)$ from continuously recorded 10-minute mean wind velocities, this assumption will not hold and uncertainties will be introduced, since adjacent recordings will likely be correlated. However, in this study the parent distribution is estimated from the extreme value distribution. The estimated extreme value distribution is uncertain, due to a low number of data, but this data is chosen as statistically independent values, so the assumption of statistical independence in Eq. (13) should hold for this approach. Estimating 100-year return periods, based on short measurement time-series, will introduce uncertainty. This is likely the main reason for the observed deviations seen in Table 5 for the westerly winds.

Table 4
Fitted probability distribution parameters and R-squared values for the mean wind velocity.

	Weibull distribution			Lognormal distribution		
	λ	k	R^2	σ	μ	R^2
East	5.1941	1.7946	0.99999	N/A	N/A	N/A
West	1.4063	0.8616	0.99872	0.4894	1.0967	0.99757

3.3. Environmental contours

The probabilistic turbulence model is established as lognormally distributed variables conditional on the mean wind velocity and wind direction. However, the mean wind velocity is usually described by a Weibull distribution and not a lognormal distribution. To establish the environmental contours for combinations of the lognormally distributed turbulence parameters and the Weibull distributed mean wind velocity using the inverse FORM technique, a combination of the Rosenblatt transformation and the linear transformation can be applied.

The mean wind velocity can be transformed first as if it was the first step of a Rosenblatt transform:

$$F_U(U) = \Phi(u_1) \;\Leftrightarrow\; U = F_U^{-1}[\Phi(u_1)] \tag{15}$$

Then, instead of taking one variable at a time using conditional CDFs as shown in Eq. (5), all the remaining lognormally distributed turbulence variables can be transformed in the same operation using the linear transformation described in Section 2, given the already transformed mean wind velocity:

$$F_{\sigma_u,\sigma_w,A_u,A_w,K_u,K_w|U}(\sigma_u, \sigma_w, A_u, A_w, K_u, K_w|\, U) \rightarrow \Phi(u_2, u_3, u_4, u_5, u_6) \tag{16}$$

In Figs. 7 and 8, the environmental contour lines for combinations of the mean wind velocity and the six turbulence parameters are shown for both easterly and westerly winds. Contour lines based directly on the transformed extreme value distribution (asymptotic) of the mean wind velocity are shown together with the contours based on the fitted parent PDFs shown in Fig. 6 (Weibull and lognormal). As Figs. 7 and 8

Table 5
Estimated 100-year return period mean wind velocities from the extreme value distribution and the fitted parent distributions.

	Extreme	Weibull	Lognormal
East	23.759	23.900	N/A
West	30.281	33.787	35.950

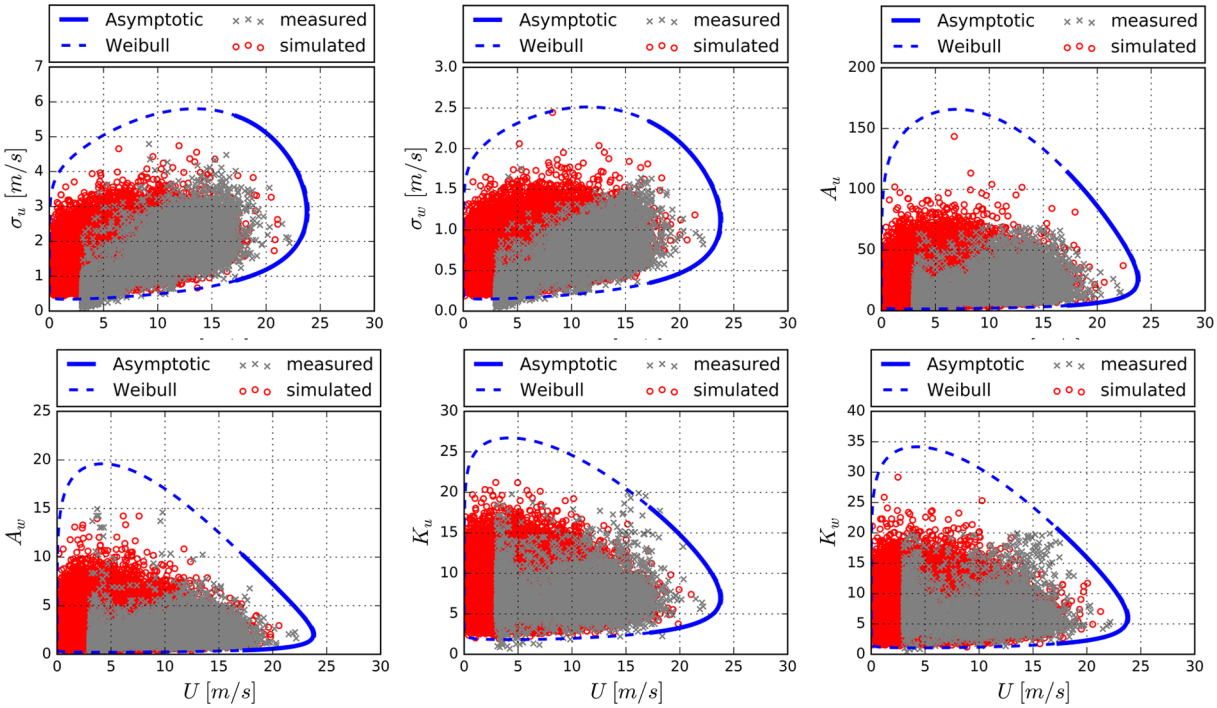

Fig. 7. Environmental contours of turbulence components and mean wind velocity for easterly winds.

show, the transformed extreme value distribution overlaps almost perfectly with the fitted parent distribution for the easterly winds, but relatively large deviations between the methods can be seen in the tail region for the westerly winds.

Figs. 7 and 8 also show the full-scale measurement data used as the basis for the probabilistic turbulence model. To illustrate the missing data in the lower mean wind velocity range due to the triggering in the measurement system, Monte Carlo simulated points from the probabilistic model are shown in the backgrounds of the plots. The number of simulated points correspond to the number of 10-minute time windows in a 4-year period ($N = 4 \times 365.25 \times 24 \times 6 = 210\,384$).

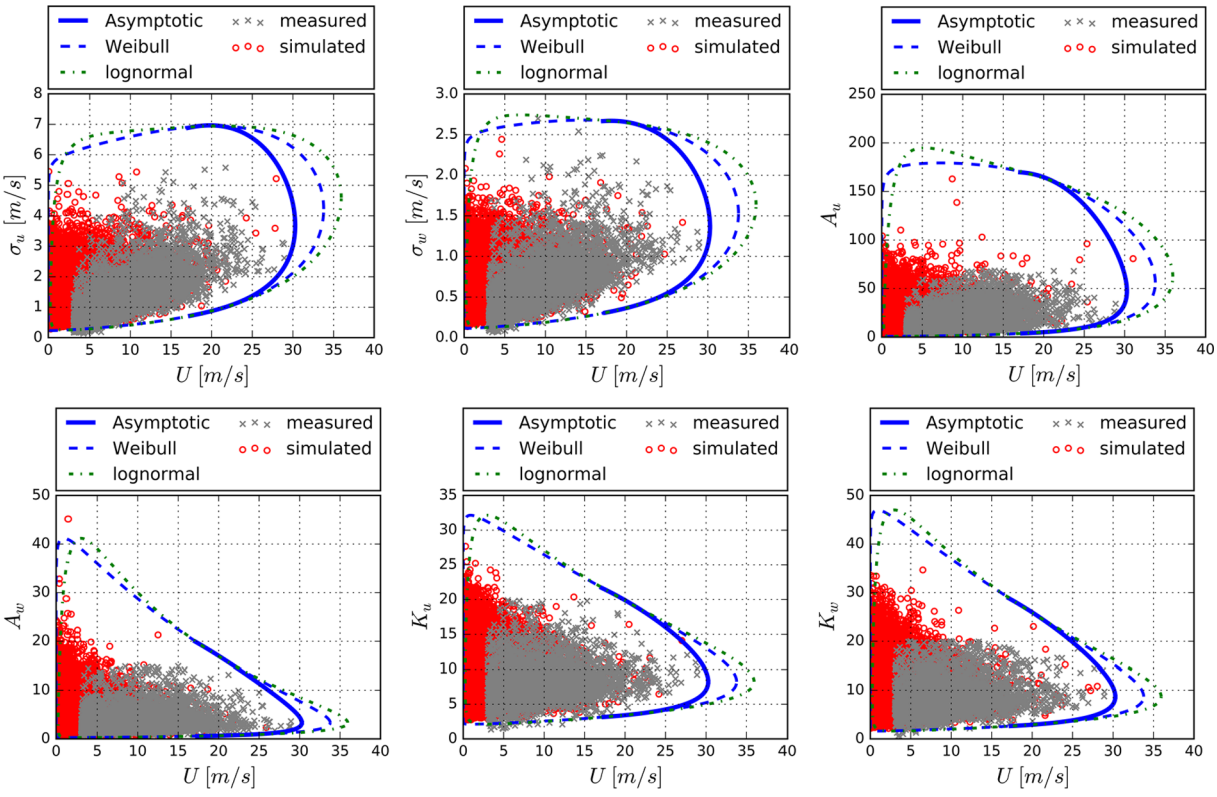

Fig. 8. Environmental contours of turbulence components and mean wind velocity for westerly winds.

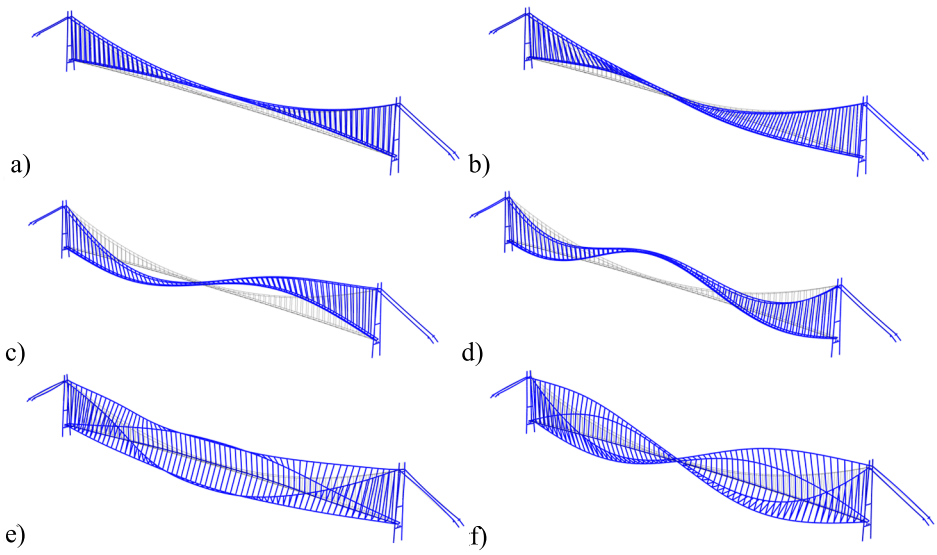

Fig. 9. Mode shapes of the Hardanger Bridge: (a) First lateral mode (19.8 s), (b) Second lateral mode (10.0 s), (c) First vertical mode (9.2 s), (d) Second vertical mode (7.1 s), (e) First torsional mode (2.8 s) and (f) Second torsional mode (1.9 s).

4. Long-term RMS buffeting response by the environmental contour method

4.1. Buffeting analysis

Buffeting response calculations of the Hardanger Bridge are performed in the frequency domain using the multimode theory, described in detail in [55–59], and implemented in the python programming language [60]. The response is calculated in normalized modal coordinates, and the response spectral density in real coordinates are achieved by the following transformation:

$$\boldsymbol{S}_r(\omega) = \boldsymbol{\Phi}(x)\boldsymbol{S}_\eta(\omega)\boldsymbol{\Phi}^T(x) \tag{17}$$

where $\boldsymbol{S}_r(\omega)$is the response spectral density matrix in real coordinates, $\boldsymbol{S}_\eta(\omega)$is the modal response spectrum, and $\boldsymbol{\Phi}(x)$is a vector containing the natural mode shapes. The structural properties of the system are based on a 3D finite element model in Abaqus [61]. From the Abaqus model it is possible to extract the section forces corresponding to a normalized deformation mode shape. By using these section force mode shapes in the transformation described by Eq. (17), the response spectral density matrix for the section forces is achieved directly. The aeroelastic self-excited forces are described based on wind tunnel experiments [62], and the structural damping ratio is chosen as 0.5% of the critical damping for all modes.

The modes affecting the considered response has been identified by convergence calculations. Considering the section forces, the first 6 lateral, the first 14 vertical, and the first 6 torsional modes are included in the calculations. For acceleration responses, all contributing modes below a cut-off frequency of 1 Hz are included in the calculations. This means that some high frequency contribution to the buffeting accelerations will be excluded, but for comparison reasons the cut-off frequency is chosen consistent with the filtering of the full-scale measurement data presented in Section 5. In Fig. 9, the first two eigenmodes in the main degrees of freedom are shown, and the natural periods of the first 15 modes are presented in Table 6, along with a description of the mode shape.

Table 6
The frequency, period and shape of the first 15 natural modes of the Hardanger Bridge.

Mode	Frequency [Hz]	Period [s]	Shape description
1	0.051	19.77	Lateral sym.
2	0.100	10.00	Lateral asym.
3	0.109	9.18	Vertical asym.
4	0.141	7.08	Vertical sym.
5	0.174	5.75	Lateral sym.
6	0.200	4.99	Vertical sym.
7	0.211	4.74	Vertical asym.
8	0.222	4.51	Cabel vibration
9	0.230	4.34	Cabel vibration
10	0.235	4.26	Cabel vibration
11	0.245	4.08	Cabel vibration
12	0.273	3.66	Vertical sym.
13	0.302	3.31	Lateral asym.
14	0.329	3.04	Vertical asym.
15	0.356	2.81	Torsional sym.

The wind field is described as a stationary stochastic process through the cross-spectral density matrix as follows:

$$\boldsymbol{S}_V(\Delta s, \omega) = \begin{bmatrix} S_{uu}(\Delta s, \omega) & S_{uw}(\Delta s, \omega) \\ S_{uw}(\Delta s, \omega) & S_{ww}(\Delta s, \omega) \end{bmatrix} \tag{18}$$

where S_{nm} represents the cross-spectral densities for the n and m components of the turbulence between two points separated in space by the distance Δs. In the current study, the off-diagonal terms of the cross-spectral density matrix are assumed to be negligible. The cross-spectral density for a single turbulence component can be described through the auto-spectral density function and the normalized cross-spectra as follows:

$$S_{nn}(\Delta s, \omega) = S_n(\omega)C_n(\Delta s, \omega) \tag{19}$$

$$C_n(\Delta s, \omega) = \exp(-\sqrt{(K_{nx}\frac{\omega\Delta x}{2\pi U})^2 + (K_{nz}\frac{\omega\Delta z}{2\pi U})^2}) \tag{20}$$

where S_n is the auto-spectral density function, C_n is the normalized cross-spectra, and K_{nx} and K_{nz} are the decay coefficients in the along-span- and vertical directions, respectively. The vertical decay coefficients will be assumed to be constant ($K_{uz} = 10$, $K_{wz} = 3$) because these are not included in the probabilistic model.

The steady-state static coefficients used in the calculations are shown in Table 7 [62]. Effects from aerodynamic admittance are neglected by setting the admittance functions to unity. From the investigations performed by [63] it was observed that by neglecting the three-dimensional admittance, consisting of the two-dimensional strip theory admittance function and the effect where the load correlation on the girder may be larger than the turbulence correlation, a slightly

Table 7
Steady-state static coefficients used in the buffeting analyses (0-degree angle of attack).

Bridge member	*Width* [m]	*Depth* [m]	C_D	C_L	C_L'	C_M	C_M'
Girder	18.3	3.33	1.050	−0.363	2.220	0.017	0.786
Main cables	0.6	0.6	1.0/0.7	0	0	0	0

conservative estimate of the aerodynamic buffeting forces could be expected. The cable drag loads have been estimated based on [64] for a painted circular cable based on a Reynolds number of approximately 1.5e6. The estimated cable drag coefficient is 1.0, but to account for some shielding effects, the drag coefficient for the downstream main cable is reduced to 0.7. Wind loads on other bridge members, such as hangers and towers, are neglected in these calculations because they are expected to have very little effect on the dynamic response of the bridge girder.

4.2. Self-excited forces

When using long-term calculation procedures such as the environmental contour method, behavior at lower mean wind velocities than what is usually considered can become interesting. A challenge arises for the self-excited forces since information about the aerodynamic derivatives (ADs) for low reduced velocities is desirable. This means that the extrapolation of the ADs outside the range where test data are available need to be handled carefully.

The self-excited forces can be written in the frequency domain as follows [65]:

$$
\begin{aligned}
q_y &= \tfrac{1}{2}\rho U^2 B\left(KP_1^*\tfrac{\dot{r}_y}{U} + KP_2^*\tfrac{B\dot{r}_\theta}{U} + K^2P_3^* r_\theta + K^2P_4^*\tfrac{r_y}{B} + KP_5^*\tfrac{\dot{r}_z}{U} + K^2P_6^*\tfrac{r_z}{B}\right)\\
q_z &= \tfrac{1}{2}\rho U^2 B\left(KH_1^*\tfrac{\dot{r}_z}{U} + KH_2^*\tfrac{B\dot{r}_\theta}{U} + K^2H_3^* r_\theta + K^2H_4^*\tfrac{r_z}{B} + KH_5^*\tfrac{\dot{r}_y}{U} + K^2H_6^*\tfrac{r_y}{B}\right)\\
q_\theta &= \tfrac{1}{2}\rho U^2 B^2\left(KA_1^*\tfrac{\dot{r}_z}{U} + KA_2^*\tfrac{B\dot{r}_\theta}{U} + K^2A_3^* r_\theta + K^2A_4^*\tfrac{r_z}{B} + KA_5^*\tfrac{\dot{r}_y}{U} + K^2A_6^*\tfrac{r_y}{B}\right)
\end{aligned}
\tag{21}
$$

where $K=(\omega B)/U$ is the reduced frequency, and r_n is the displacement motions. Zasso [66] proposed a convention where the ADs were fitted to the test data using the force components (aerodynamic derivative multiplied with the K or K^2 for the damping and stiffness ADs, respectively) going directly into Eq. (21), as shown in Figs. 10a and 11a. This would re-scale the amplitude of the AD's making them more similar throughout the reduced frequency range, compared with the Scanlan convention [65]. Extrapolations outside the reduced velocity range where test data are available is a challenge since no physical model is available. In this work, this extrapolation was performed by keeping the force component constant outside the test range. This choice is made by a lack of good alternatives, but in this way, the extrapolations are controlled, and the extrapolated ADs display a physical behavior toward the low reduced-velocity range for the important ADs. It should be noted that the convention used here only differs from the Scanlan convention in the domain where the AD model is fitted to the test data, and the mathematical modelling of the forces will be equivalent.

In Figs. 10 and 11, the aerodynamic derivatives from the wind tunnel tests performed by [62] are plotted together with fitted 2nd order polynomial functions. The polynomials are fitted to the format of force components going directly into Eq. (21), as shown in Figs. 10a and 11a. The resulting ADs plotted in the classical format are shown in Figs. 10b and 11b.

4.3. Section-moment buffeting response on the contours

In this section, the section-moment standard deviations from the buffeting action of the Hardanger Bridge girder are investigated as functions of the mean wind velocity and turbulence parameters. In Fig. 12, the response spectral densities of the section moments are shown for all positions along the bridge girder.

To find the critical environmental load situation for a considered response quantity, combinations of environmental variables on the contour can be picked based on engineering judgment and manual iterations, or it can be found automatically using numerical optimization. For environmental contour lines based on only two stochastic variables, it can be relatively simple to find the critical combination using only a few manual iterations, but for contour surfaces with 3 variables or contour manifolds with more than 3 variables, it becomes increasingly challenging to identify the critical combinations manually.

A challenge with numerical optimization is separating local from global maxima on the optimized function. For the cases investigated in this work, local maxima on the response function are not expected, and simple optimization algorithms should be sufficient. However, the

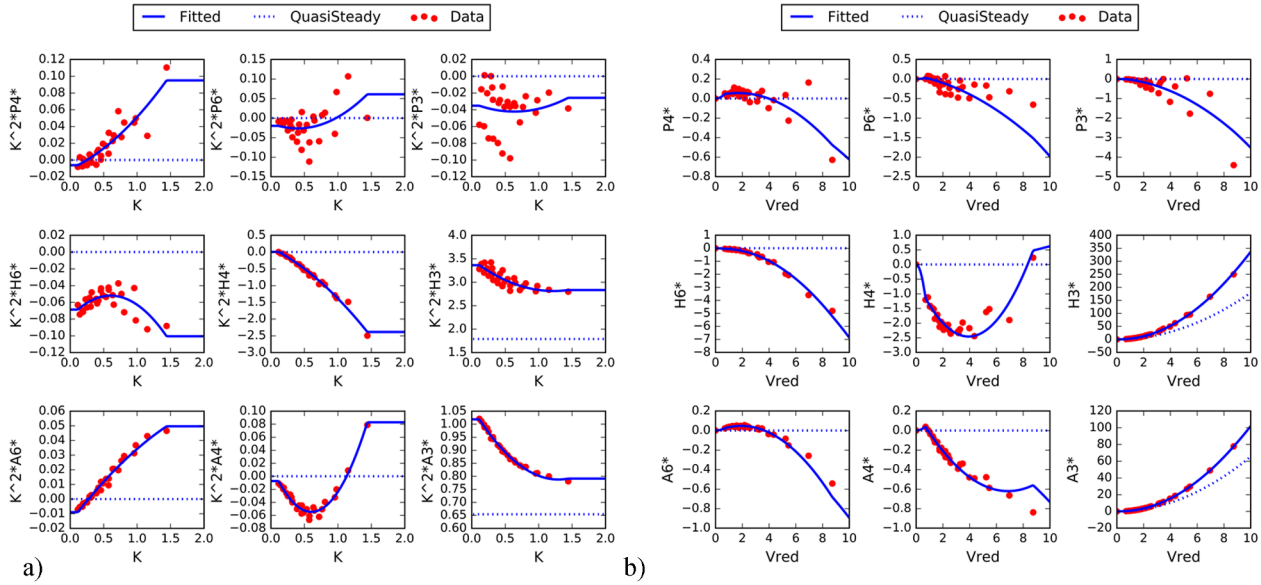

Fig. 10. Fitted polynomial functions for the stiffness-related aerodynamic derivatives: (a) force component format ($K=(\omega B)/U$) and (b) classical format ($Vred = U/\omega B$).

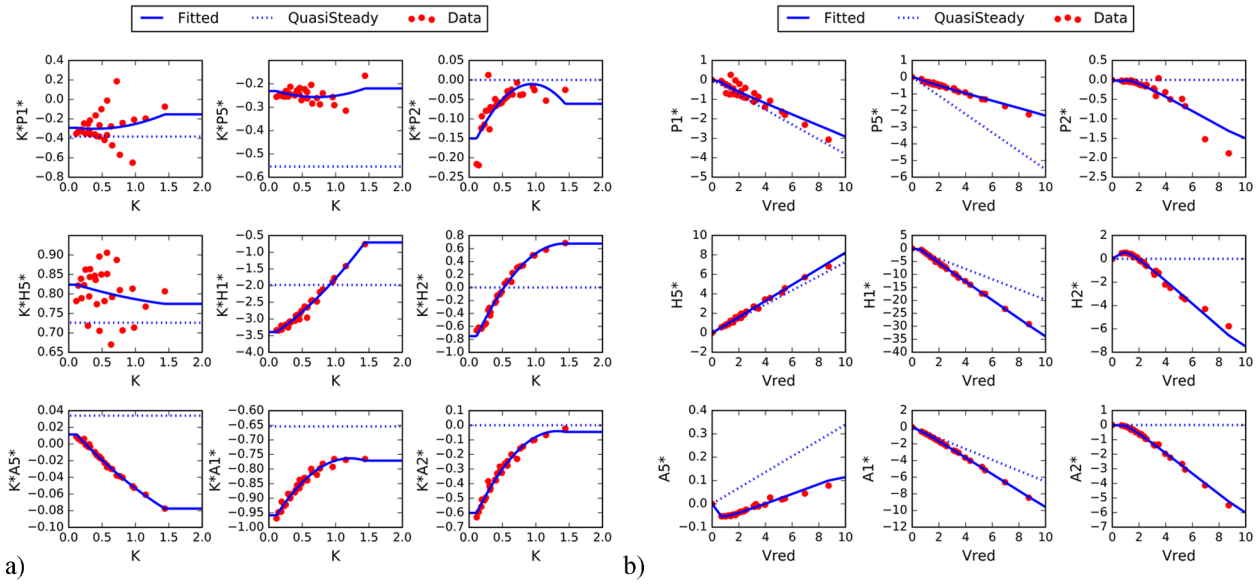

Fig. 11. Fitted polynomial functions for the damping-related aerodynamic derivatives: a) force component format ($K = (\omega B)/U$) and b) classical format ($Vred = U/\omega B$).

optimization algorithms need to be constrained to only find solutions on the environmental contour. The optimization algorithm used in this study is the sequential least-squares programming method (SLSQP) [67]. This algorithm can be used with boundary constraints as well as user-defined constraint functions.

Objective function:

The function to be optimized is the short-term response calculation as a function of the environmental variables:

$$response = f(\boldsymbol{X}) \tag{22}$$

where $\mathbf{X} = [v_1, v_2, v_3, \ldots, v_n]$ and v_i are the environmental variables.

Constraint function:

The constraint demands that all accepted combinations of **X** should be on the environmental contour-line, surface, or manifold, depending on the number of variables included, for a given statistical return period. The constraint function needs to transform the variables into the standard normal space and check if they refer to points with the target distance to the origin, namely the reliability index, β, as follows:

$$|\boldsymbol{Y}| - \beta = 0 \tag{23}$$

where $\mathbf{Y} = [u_1, u_2, u_3, \ldots, u_n]$ and u_i are the standard normal uncorrelated variables.

The quarter-span RMS weak- and strong-axis moments (σ_{sm1} and σ_{sm2}, respectively), as well as the torsional moment (σ_{sm3}) in the girder, is calculated along the contour lines for combinations of the mean wind velocity and the different turbulence parameters. The variation in RMS response along the contour lines based on direct transformation from the extreme value distribution is shown in Figs. 13 and 14. In these plots, the mean wind velocity together with one turbulence parameter is described with the environmental contour method, while the other turbulence parameters are chosen to correspond to the tips of the contours, the case of maximum mean wind velocity. The position on the contour line with the highest buffeting response is indicated with a star in the plots. The RMS response and the environmental variables corresponding to this position are shown in Tables 8 and 9. In the backgrounds of Figs. 13 and 14, isoresponse lines corresponding to constant response as a function of the mean wind velocity and the turbulence parameter under consideration are shown. If the isoresponse lines are straight and vertical, the investigated buffeting response is not sensitive to variation in the turbulence parameter under consideration, but if the lines are inclined, the turbulence parameter is important.

The turbulence standard deviations are the most influential parameters on the investigated buffeting response. The along-wind turbulence standard deviation (σ_u) has a significant effect on the weak- and strong-axis moments in the girder quarter spans but little effect on the torsional moment response. The vertical turbulence standard deviation (σ_w) has a large effect on the weak-axis moment and the torsional moment but less effect on the strong-axis moment.

From Figs. 13 and 14, it can be seen from the isoresponse lines that the response is sensitive to the decay coefficients ($K_{u,w}$), but since the contour lines become narrow toward the high wind speeds, the effect on the design response is less significant. The section-moment buffeting

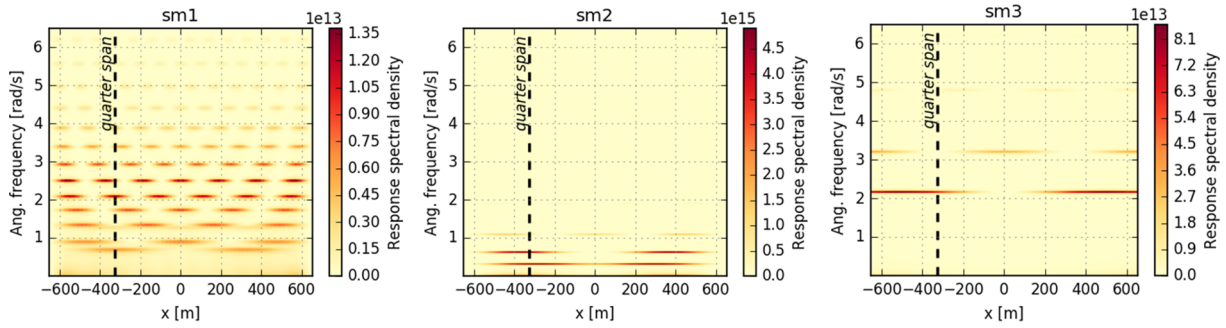

Fig. 12. Response spectral density of the weak axis (sm1), strong axis (sm2) and torsional moment (sm3) for a 30 m/s mean wind velocity case with design basis turbulence definition.

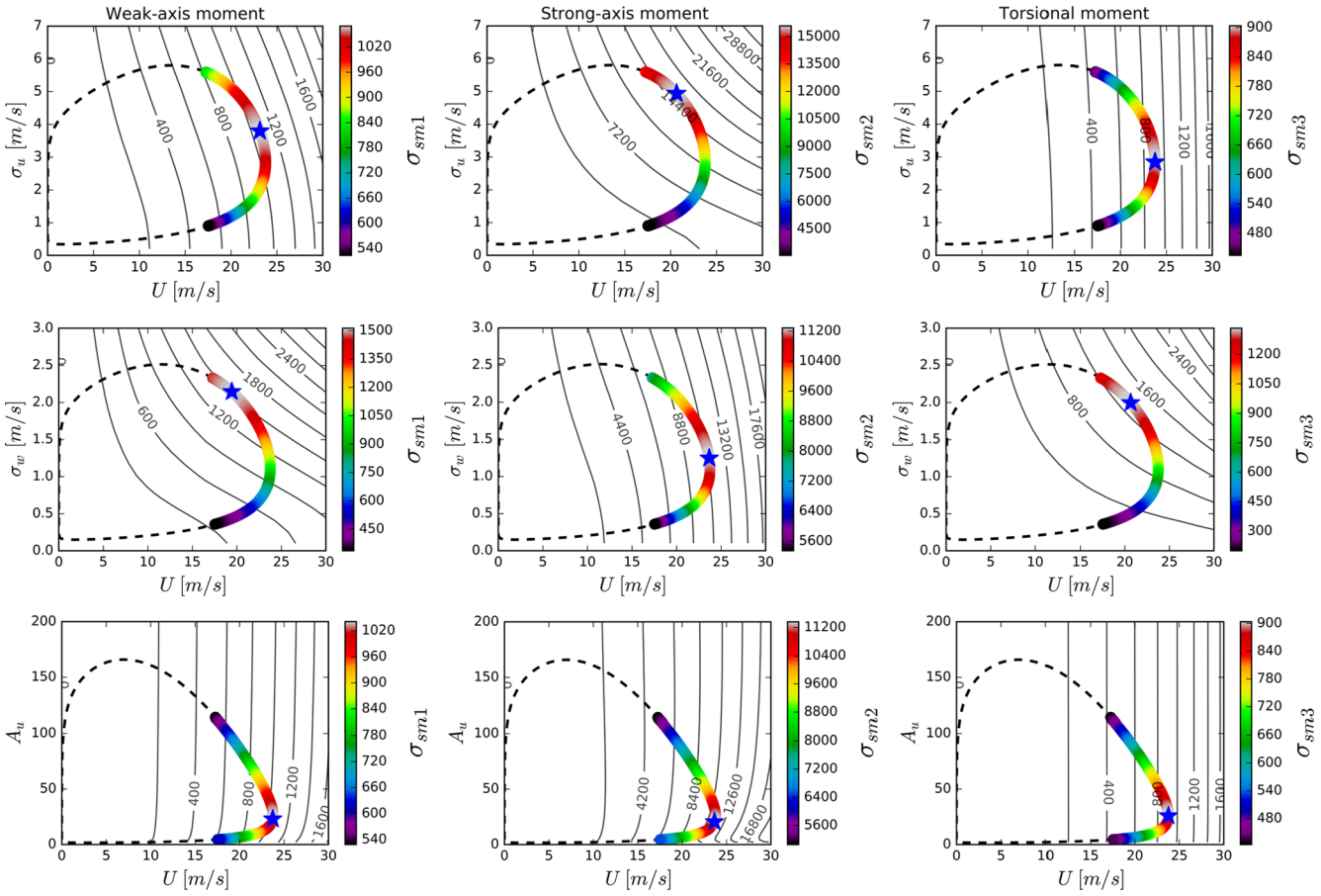

Fig. 13. Buffeting RMS response of weak-axis (sm1), strong-axis (sm2) and torsional moments (sm3) [kNm] along contours for the turbulence components and mean wind velocity for easterly wind, where the larges response is indicated with a blue star marker, and isoresponse lines are shown in the background.

responses of the Hardanger Bridge are not very sensitive to variation in the nondimensional spectral parameters ($A_{u,w}$), but it should be noted that bridges with even lower eigenfrequencies may be more sensitive to variations in these parameters.

In Figs. 15 and 16, the two turbulence parameters most influential to the section moment RMS responses are combined with the mean wind velocity in three-dimensional contour surfaces. The most critical turbulence parameters for the section moments are identified from the two-dimensional contours in Tables 8 and 9 as follows:

- Weak-axis moment, *sm1*; the along-wind and vertical turbulence standard deviations ($\sigma_{u,w}$),
- Strong-axis moment, *sm2*; the along-wind turbulence standard deviation (σ_u) and the along-wind turbulence decay coefficient (K_u),
- Torsional moment, *sm3*; the vertical turbulence standard deviation (σ_w) and the vertical turbulence decay coefficient (K_w).

The maximum response standard deviations and the three-dimensional contour surfaces and seven-dimensional contour manifolds, including all the turbulence parameters, are predicted using constrained numerical optimization and summarized in Tables 10 and 11. The results show significant effects from the turbulence variability on the design environmental conditions for the Hardanger Bridge, with an increased response of up to ~60% when comparing the critical point on the environmental contour surface with the point of the maximum mean wind velocity.

5. Comparison with full-scale response measurements

In Fig. 17, the 10-minute average measured midspan lateral-, vertical- and torsional acceleration RMS responses are shown for the westerly and easterly wind directions for the Hardanger Bridge. The high frequency contribution to the acceleration measurements was removed from the data by low-pass filtering the recorded response with a cut-off frequency of 1 Hz. The traffic density on the Hardanger Bridge is relatively low, and by filtering out the high frequency content, negligible effects from traffic loading are expected for the strong wind acceleration responses. For more information about the processing of the acceleration measurements, the reader is referred to [2].

The measured scatter points are colored based on data density multiplied by the mean wind velocity squared. A second-order polynomial function is fitted to the measurements, as shown in Fig. 17. Using the deterministically chosen design basis turbulence parameters from Table 3, the acceleration responses are calculated and plotted in Fig. 17. Comparing these lines obtained from the design basis values with the measured response shows the limitations of the traditional design methodology, which is unable to describe the scattered response observed from the measurements.

An upper and lower bound for the acceleration response was calculated as a function of the mean wind velocity using the environmental contour method to investigate how the measured midspan acceleration response corresponds with the response predictions. These estimates were calculated by finding the maximum and minimum responses on a 100-year return period environmental contour surface constrained to a given mean wind velocity. Thus, for each considered mean wind velocity, a point for the upper and lower bound lines was identified. The environmental contour bounds were based on contour surfaces from the mean wind velocity together with the following turbulence parameters:

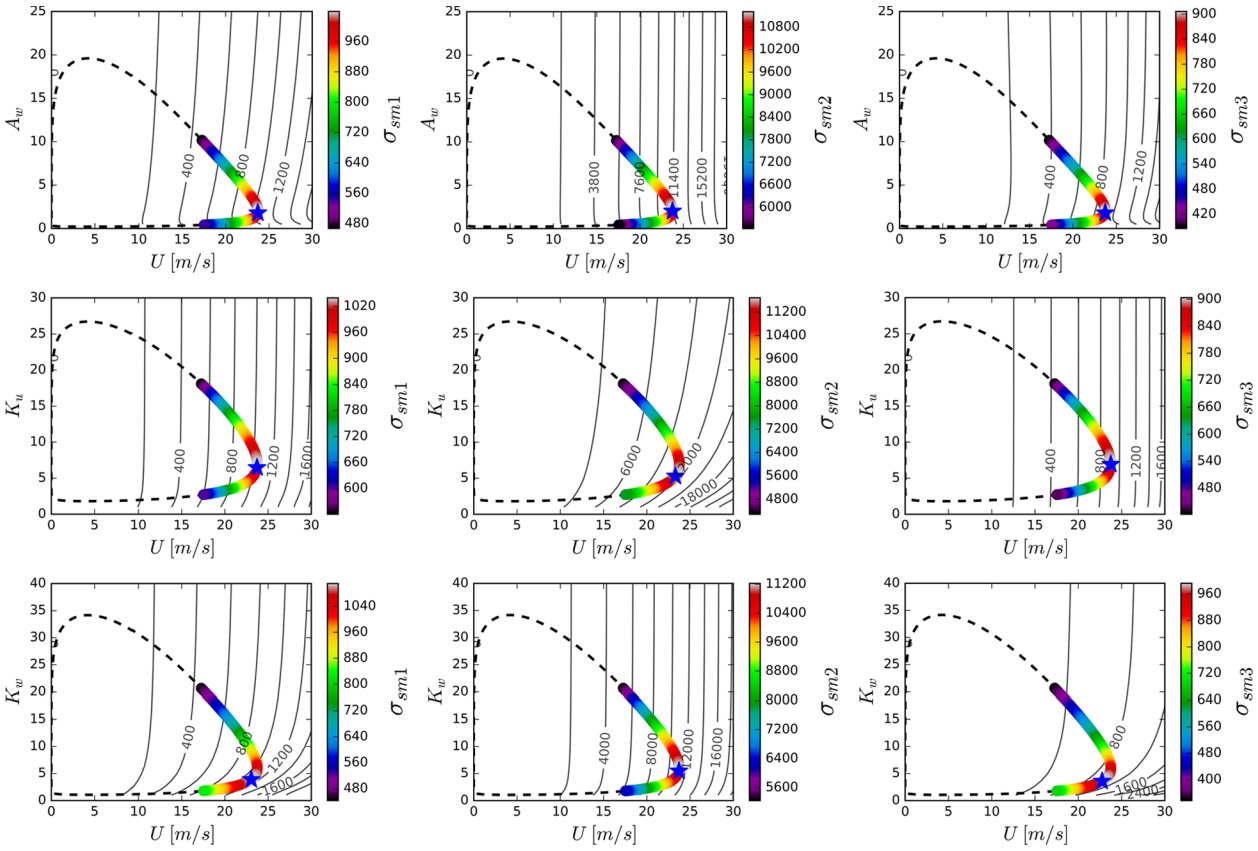

Fig. 13. (*continued*)

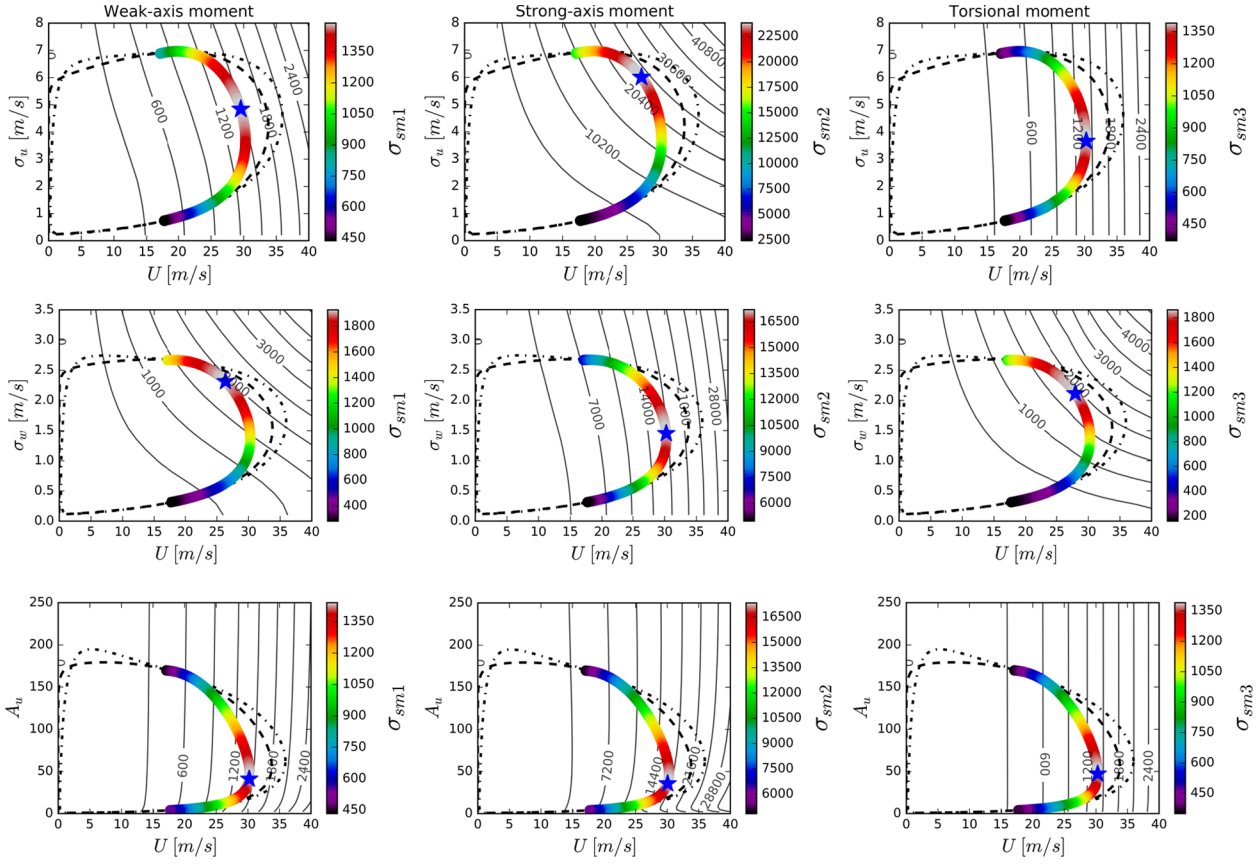

Fig. 14. Buffeting RMS response of weak-axis (sm1), strong-axis (sm2) and torsional moments (sm3) [kN m] along contours for the turbulence components and mean wind velocity for westerly winds, where the larges response is indicated with a blue star marker, and isoresponse lines are shown in the background.

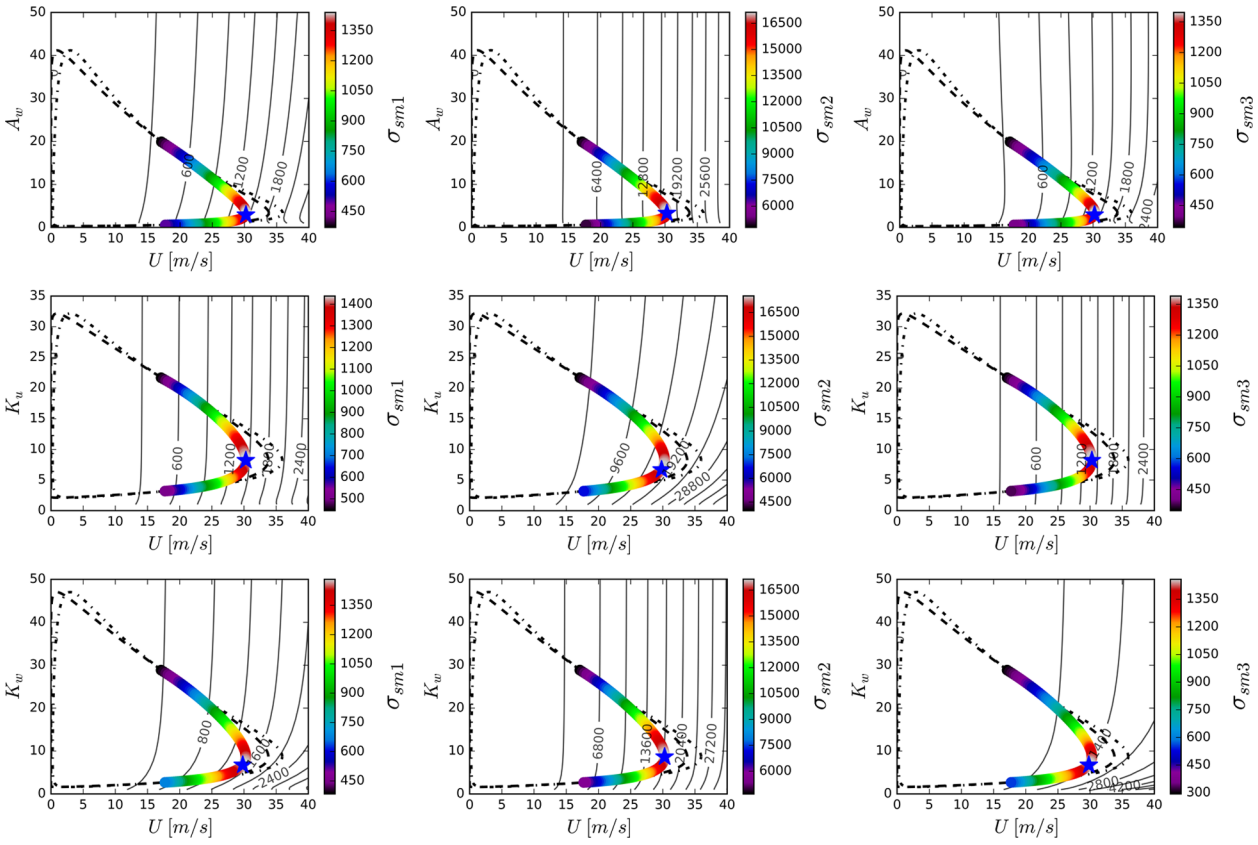

Fig. 14. (*continued*)

- Horizontal acceleration, *a2*; the along-wind turbulence standard deviation (σ_u) and the along-wind turbulence decay coefficient (K_u),
- Vertical acceleration, *a3*; the along-wind and vertical turbulence standard deviations ($\sigma_{u,w}$),
- Torsional acceleration, *ar1*; the vertical turbulence standard deviation (σ_w) and the vertical turbulence decay coefficient (K_w).

As shown in Fig. 17, the acceleration response bounds predicted by the environmental contour method eclipse most of the measured scatter for all response quantities and both wind directions. These bounds are based on the 100-year return period environmental contours and compared with approximately 4 years of measurement data. Theoretically, all measurement data should lie within these bounds, but uncertainties in the probabilistic turbulence model, the buffeting calculations and the simplification where only the two most important turbulence parameters are included in the environmental contours may affect these results.

When considering the horizontal acceleration, the trend in the scatter is followed very well for both wind directions, but especially for the easterly winds, the bounds are too narrow to be able to eclipse the full scatter of the measurement data. Limitations in the probabilistic turbulence model, such as omitting the angle of attack, may affect the predicted response. Additionally, other assumptions made in the buffeting calculations, such as the assumption of stationarity, may affect the results.

The vertical acceleration response bounds cover the measured scatter data very well for both wind directions. In addition to uncertainties regarding the probabilistic turbulence model and simplifications in the buffeting calculations, some uncertainty from the self-excited forces is introduced for the vertical acceleration response. The midspan acceleration response spectral densities normalized with the maximum response spectrum amplitude for each mean wind velocity are shown in Fig. 18. The reduced velocity range where aerodynamic derivative test data are available is indicated in the plots. For the vertical acceleration response, many contributions come from the reduced velocity range extrapolated from the AD test range. This introduces some uncertainty into the vertical acceleration response estimates.

When considering the torsional response, the predicted torsional

Table 8
Maximum RMS section moments in the girder quarter span from contour lines based on the mean wind velocity and one turbulence parameter for easterly winds. The percentage of increased response compared with the event of the maximum mean wind speed ($U = 23.76$ *m/s*, $\sigma_u = 2.84$ *m/s*, $\sigma_w = 1.10$ *m/s*, $A_u = 25.8$, $A_w = 2.01$, $K_u = 6.92$, $K_w = 5.98$) is indicated.

Contour variables	U *m/s*	*Turb Var*	σ_{sm1} *kN m*	*%*	U *m/s*	*Turb Var*	σ_{sm2} *kN m*	*%*	U *m/s*	*Turb Var*	σ_{sm3} *kN m*	*%*
U	23.76	–	1039	0	23.76	–	11,206	0	23.76	–	903	0
U, σ_u	23.13	3.80 *m/s*	1070	3	20.64	4.94 *m/s*	15,580	39	23.76	2.84 *m/s*	903	0
U, σ_w	19.43	2.15 *m/s*	1513	46	23.67	1.25 *m/s*	11,284	1	20.64	2.00 *m/s*	1333	48
U, A_u	23.73	23.0	1041	0	23.64	20.5	11,358	1	23.76	25.8	903	0
U, A_w	23.73	1.80	1039	0	23.76	2.02	11,206	0	23.73	1.80	906	0
U, K_u	23.73	6.47	1039	0	23.31	5.30	11,688	4	23.76	6.92	903	0
U, K_w	23.06	3.89	1110	7	23.73	5.48	11,221	0	22.76	3.58	992	10

Table 9
Maximum RMS section moments in the girder quarter span from contour lines based on the mean wind velocity and one turbulence parameter for westerly winds. The percentage of increased response compared with the event of the maximum mean wind speed (U = 30.30 m/s, σ_u = 3.66 m/s, σ_w = 1.36 m/s, A_u = 47.1, A_w = 3.32, K_u = 8.21, K_w = 8.65) is indicated.

Contour variables	U m/s	Turb Var	σ_{sm1} kN m	%	U m/s	Turb Var	σ_{sm2} kN m	%	U m/s	Turb Var	σ_{sm3} kN m	%
U	30.28	–	1437	0	30.28	–	17,131	0	30.28	–	1390	0
U, σ_u	29.55	4.84 m/s	1488	4	27.20	6.01 m/s	23,821	39	30.28	3.66 m/s	1390	0
U, σ_w	26.36	2.32 m/s	1928	34	30.25	1.45 m/s	17,198	0	27.94	2.11 m/s	1865	34
U, A_u	30.22	41.1	1440	0	30.07	35.7	17,337	1	30.28	47.1	1390	0
U, A_w	30.22	2.93	1440	0	30.28	3.32	17,131	0	30.22	2.93	1396	0
U, K_u	30.28	8.21	1437	0	29.81	6.70	17,555	2	30.28	8.21	1390	0
U, K_w	29.81	6.73	1483	3	30.28	8.65	17,131	0	29.81	6.73	1458	5

accelerations seem to be strongly overpredicted for both wind directions. Almost all the contributions to the response are based on self-excited forces outside the reduced velocity AD test range, except for the very high mean wind velocities. Along with sensitivity to the static coefficients, this will introduce significant uncertainty to these predictions.

6. Conclusions

Turbulence uncertainty effects on the buffeting response of the Hardanger Bridge girder have been investigated using the environmental contour method. The results show large effects on the predicted response and potential for substantial improvements to the current

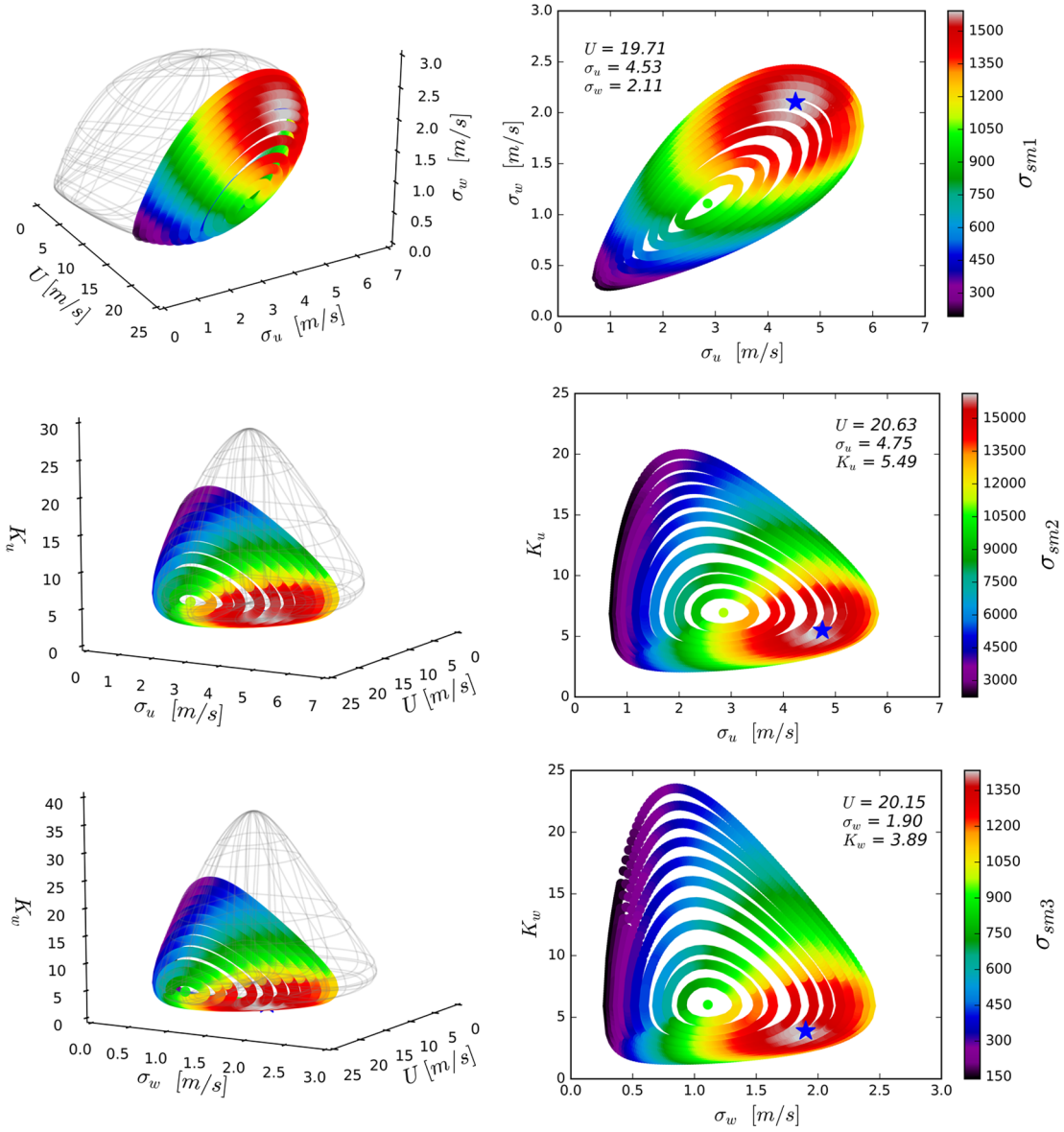

Fig. 15. Buffeting RMS response of weak-axis (sm1), strong-axis (sm2) and torsional moments (sm3) [kN m] on contour surfaces for the turbulence components and mean wind velocity for easterly wind, where the larges response is indicated with a blue star marker.

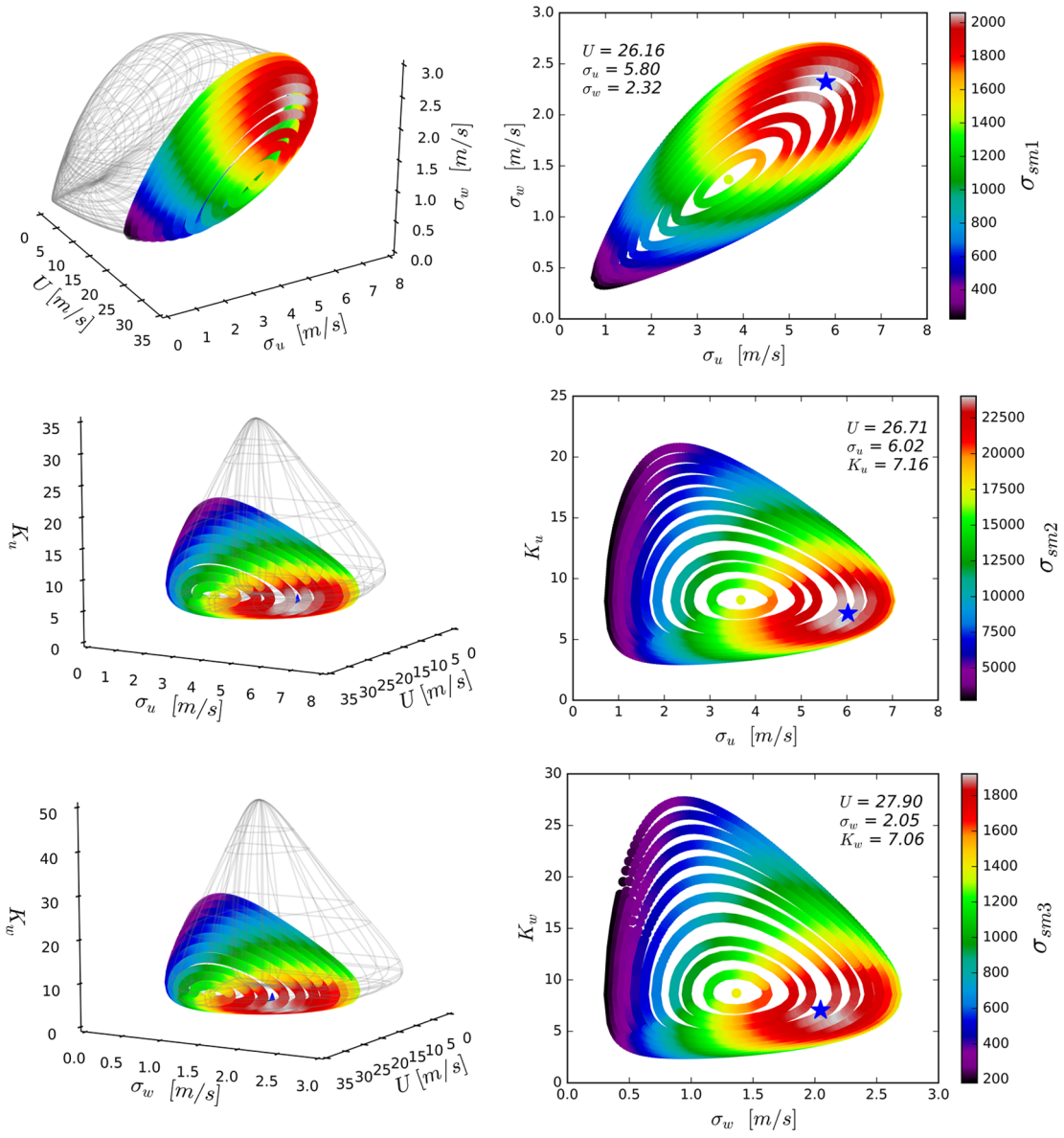

Fig. 16. Buffeting RMS response of weak-axis (sm1), strong-axis (sm2) and torsional moments (sm3) [kN m] on contour surfaces for the turbulence components and mean wind velocity for westerly winds, where the larges response is indicated with a blue star marker.

design methodology. The following conclusions can be drawn:

- By describing the turbulence parameters with lognormal distributions, the transformation between the standard normal space and the real space is practically achievable for multiple variables even with a limited amount of measurement data.
- Numerical optimization algorithms constrained to find solutions on the environmental contour were successfully used in the investigations presented in this paper. The method is especially suitable when the number of environmental variables exceeds two.
- The knowledge that the critical environmental situations will be in the tail of the mean wind velocity marginal distribution can be used

Table 10
Easterly winds maximum RMS section moments in the girder quarter span identified from numerical optimization on the environmental contours considering interesting turbulence parameter combinations. The percentage of increased response compared with the event of the maximum mean wind speed is indicated.

Contour variables	U m/s	σ_u m/s	σ_w m/s	A_u –	A_w –	K_u –	K_w –	σ_{sm1} kN m	%	σ_{sm2} kN m	%	σ_{sm3} kN m	%
U	23.76	2.84	1.10	25.8	2.01	6.92	5.98	1039	0	11,206	0	903	0
U, σ_u, σ_w	19.71	4.53	2.11	25.8	2.01	6.92	5.98	1599	54	–	–	–	–
U, σ_u, K_u	20.63	4.75	0.96	25.8	2.01	5.49	5.98	–	–	16,232	45	–	–
U, σ_w, K_w	20.15	2.41	1.90	25.8	2.01	6.92	3.89	–	–	–	–	1438	59
All	19.26	4.33	2.00	22.4	2.32	6.11	3.93	1683	62	–	–	–	–
All	20.51	4.70	1.74	25.8	2.09	5.47	5.14	–	–	16,716	49	–	–
All	20.27	4.08	1.87	23.3	2.29	6.22	3.90	–	–	–	–	1418	57

Table 11
Westerly winds maximum RMS section moments in the girder quarter span identified from numerical optimization on the environmental contours considering interesting turbulence parameter combinations. The percentage of increased response compared with the event of the maximum mean wind speed is indicated.

Contour variables	U m/s	σ_u m/s	σ_w m/s	A_u –	A_w –	K_u –	K_w –	σ_{sm1} kNm	%	σ_{sm2} kNm	%	σ_{sm3} kNm	%
U	30.3	3.66	1.36	47.1	3.32	8.21	8.65	1437	0	17,131	0	1390	0
U, σ_u, σ_w	26.2	5.80	2.32	47.1	3.32	8.21	8.65	2070	44	–	–	–	–
U, σ_u, K_u	26.7	6.02	1.20	47.1	3.32	7.16	8.65	–	–	24,431	43	–	–
U, σ_w, K_w	27.9	3.37	2.05	47.1	3.32	8.21	7.06	–	–	–	–	1929	39
All	25.9	5.64	2.26	37.7	3.69	7.46	6.96	2112	47	–	–	–	–
All	26.4	5.94	2.12	47.3	3.24	7.07	7.73	–	–	24,830	45	–	–
All	27.9	5.12	2.03	41.1	3.74	7.60	7.06	–	–	–	–	1910	37

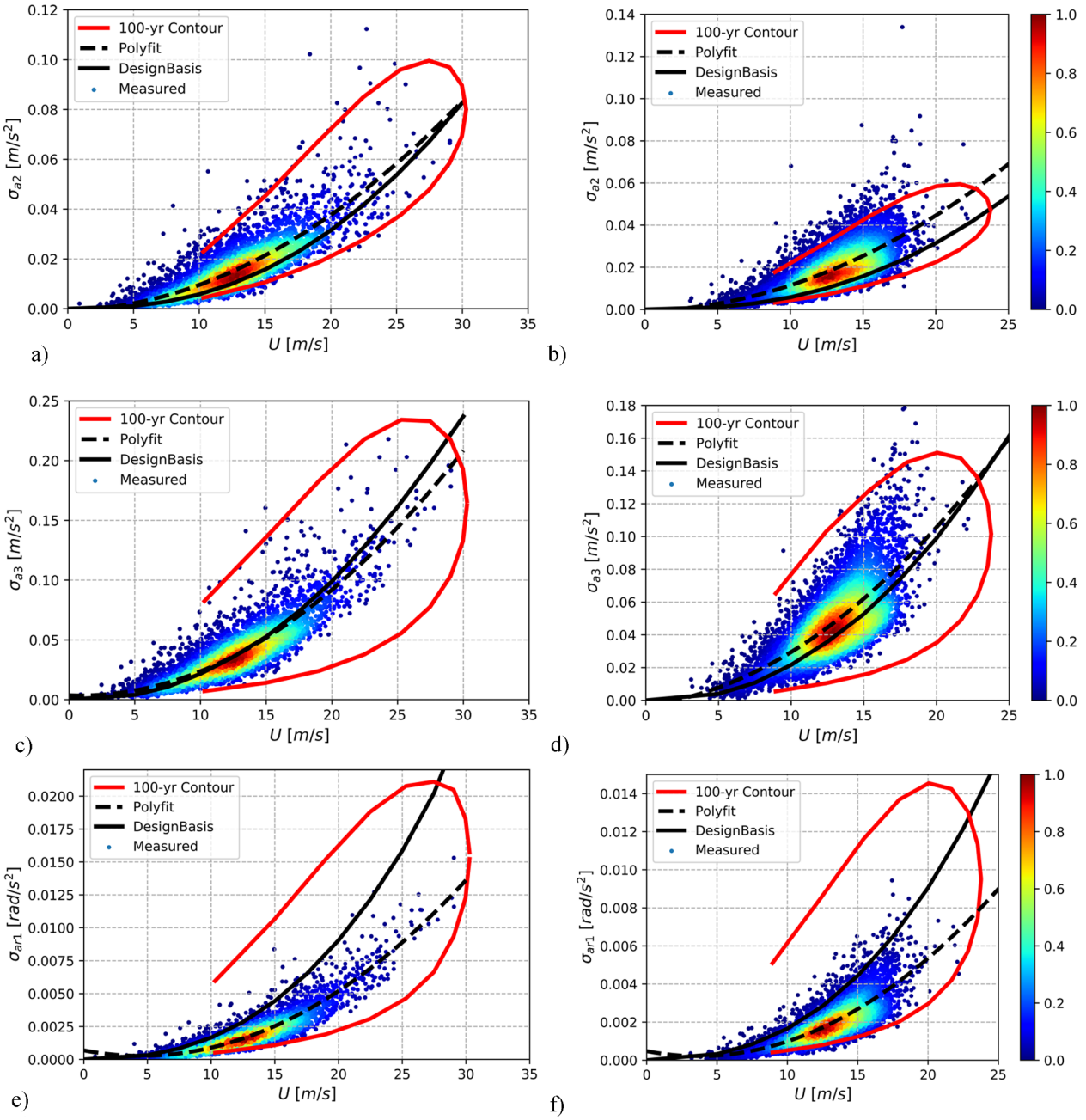

Fig. 17. Calculated and measured RMS girder acceleration response at the midspan with color bar indicating data density multiplied by U^2: (a) westerly winds lateral response, (b) easterly winds lateral response, (c) westerly winds vertical response, (d) easterly winds vertical response, (e) westerly winds torsional response and (f) easterly winds torsional response.

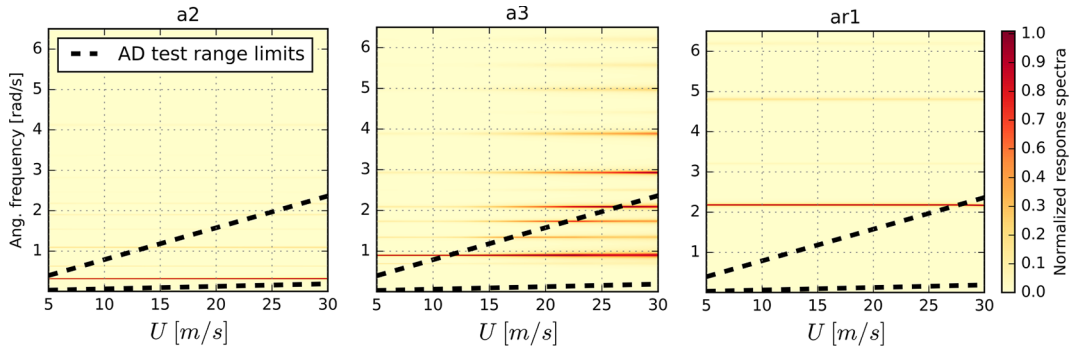

Fig. 18. Acceleration response spectral density, normalized on the maximum value for each wind speed, and AD test range indication.

as an advantage to focus the effort on fitting the PDF in the extreme tail region. Asymptotic extreme value theory was used in this work to transform the fitted extreme value distribution to the parent distribution form to achieve an enhanced marginal PDF estimate for the important range of mean wind velocities.

- Including the variability in the turbulence parameters by using the environmental contour method indicated significant effects on the important section moments for the Hardanger Bridge girder. Compared with the point on the contour with maximum mean wind velocity, an increased design response of up to ~60% was found.
- By estimating an upper and lower bound response using the environmental contour method, the scattered acceleration response measurements from the Hardanger Bridge were eclipsed, showing significant improvements to the traditional design methodology.
- The findings in this paper indicate that long-term response calculation methods, including the turbulence parameters as stochastic variables, should be considered for long-span bridges where the buffeting response is expected to significantly affect the structural reliability.

CRediT authorship contribution statement

Tor M. Lystad: Conceptualization, Methodology, Software, Formal analysis, Writing - original draft, Writing - review & editing, Visualization. **Aksel Fenerci:** Validation, Investigation, Data curation. **Ole Øiseth:** Conceptualization, Supervision, Project administration.

Declaration of Competing Interest

The authors declare that they have no known competing financial interests or personal relationships that could have appeared to influence the work reported in this paper.

Acknowledgments

Funding: The research presented in this paper has been financed by Norconsult AS, The Norwegian Public Roads Administration (NPRA) and The Research Council of Norway.

References

[1] Dunham KK. Coastal Highway Route E39 – Extreme Crossings. Transp Res Procedia 2016;14:494–8. https://doi.org/10.1016/J.TRPRO.2016.05.102.
[2] Fenerci A, Øiseth O, Rönnquist A. Long-term monitoring of wind field characteristics and dynamic response of a long-span suspension bridge in complex terrain. Eng Struct 2017;147:269–84. https://doi.org/10.1016/j.engstruct.2017.05.070.
[3] Fenerci A, Øiseth O. Measured buffeting response of a long-span suspension bridge compared with numerical predictions based on design wind spectra. J Struct Eng 2017;143. https://doi.org/10.1061/(ASCE)ST.1943-541X.0001873.
[4] Fenerci A, Øiseth O. Strong wind characteristics and dynamic response of a long-span suspension bridge during a storm. J Wind Eng Ind Aerodyn 2018;172:116–38. https://doi.org/10.1016/j.jweia.2017.10.030.
[5] Fenerci A, Øiseth O. Site-specific data-driven probabilistic wind field modeling for the wind-induced response prediction of cable-supported bridges. J Wind Eng Ind Aerodyn 2018;181:161–79. https://doi.org/10.1016/J.JWEIA.2018.09.002.
[6] Lystad TM, Fenerci A, Øiseth O. Evaluation of mast measurements and wind tunnel terrain models to describe spatially variable wind field characteristics for long-span bridge design. J Wind Eng Ind Aerodyn 2018;179:558–73. https://doi.org/10.1016/J.JWEIA.2018.06.021.
[7] Lystad TM, Fenerci A, Øiseth O. Aerodynamic effect of non-uniform wind profiles for long-span bridges. Proc. XV Conf. Ital. Assoc. Wind Eng. Springer; 2018. p. 427–39.
[8] Brownjohn JMW, Bocciolone M, Curami A, Falco M, Zasso A. Humber bridge full-scale measurement campaigns 1990–1991. J Wind Eng Ind Aerodyn 1994;52:185–218. https://doi.org/10.1016/0167-6105(94)90047-7.
[9] Miyata T, Yamada H, Katsuchi H, Kitagawa M. Full-scale measurement of Akashi-Kaikyo Bridge during typhoon. J Wind Eng Ind Aerodyn 2002;90:1517–27. https://doi.org/10.1016/S0167-6105(02)00267-2.
[10] Macdonald JHG. Evaluation of buffeting predictions of a cable-stayed bridge from full-scale measurements. J Wind Eng Ind Aerodyn 2003;91:1465–83. https://doi.org/10.1016/J.JWEIA.2003.09.009.
[11] Wang H, Li A, Guo T, Xie J. Field measurement on wind characteristic and buffeting response of the Runyang Suspension Bridge during typhoon Matsa. Sci China, Ser E Technol Sci 2009;52:1354–62. https://doi.org/10.1007/s11431-008-0238-y.
[12] Wang H, Asce M, Tao T, Asce SM, Gao Y, Xu F. Measurement of Wind Effects on a Kilometer-Level Cable-Stayed Bridge during Typhoon Haikui. J Struct Eng 2018;144:1–23. https://doi.org/10.1061/(ASCE)ST.1943-541X.0002138.
[13] Cheynet E, Bogunovic Jakobsen J, Snæbjörnsson J. Buffeting response of a suspension bridge in complex terrain. Eng Struct 2016;128:474–87. https://doi.org/10.1016/J.ENGSTRUCT.2016.09.060.
[14] Meng X, Nguyen DT, Xie Y, Owen JS, Psimoulis P, Ince S, et al. Design and implementation of a new system for large bridge monitoring—geoshm. Sensors 2018;18. http://doi.org/10.3390/s18030775.
[15] Stephen GA, Brownjohn JMW, Taylor CA. Measurements of static and dynamic displacement from visual monitoring of the Humber Bridge. Eng Struct 1993;15:197–208. https://doi.org/10.1016/0141-0296(93)90054-8.
[16] Mao J-X, Wang H, Feng D-M, Tao T-Y, Zheng W-Z. Investigation of dynamic properties of long - span cable - stayed bridges based on one - year monitoring data under normal operating condition. Struct Control Heal Monit 2018;25:1–19. https://doi.org/10.1002/stc.2146.
[17] Wang H, Hu R, Xie J, Tong T, Li A. Comparative study on buffeting performance of Sutong Bridge based on design and measured spectrum. J Bridg Eng 2013;18:587–600. https://doi.org/10.1061/(ASCE)BE.1943-5592.0000394.
[18] Naess A, Moan T. Stochastic Dynamics of Marine Structures. Cambridge University Press; 2013. http://doi.org/10.1017/CBO9781139021364.
[19] Winterstein SR, Haver S. Environmental Parameters For Extreme Response : Inverse FORM with Omission Factors. Proc 6th Int. Conf Struct. Saf. Reliab., Innsbruck, Austria: 1993.
[20] Haver S, Kleiven G. Environmental Contour Lines for Design Purposes: Why and When? 23rd Int. Conf. Offshore Mech. Arct. Eng. Vol. 1, Parts A B, 2004, p. 337–45. http://doi.org/10.1115/OMAE2004-51157.
[21] Bang Huseby A, Vanem E, Natvig B. A new approach to environmental contours for ocean engineering applications based on direct Monte Carlo simulations. Ocean Eng 2013;60:124–35. https://doi.org/10.1016/J.OCEANENG.2012.12.034.
[22] Vanem E. A comparison study on the estimation of extreme structural response from different environmental contour methods. Mar Struct 2017;56:137–62. https://doi.org/10.1016/j.marstruc.2017.07.002.
[23] Chai W, Leira BJ. Environmental contours based on inverse SORM. Mar Struct 2018;60:34–51. https://doi.org/10.1016/J.MARSTRUC.2018.03.007.
[24] Moriarty PJ, Holley WE, Butterfield S. Effect of trbulence variation on extreme loads prediction for wind turbines. J Sol Energy Eng 2002;124:387–95. https://doi.org/10.1115/1.1510137.
[25] Fitzwater LM, Cornell CA, Veers PS. Using environmental contours to predict extreme events on wind turbines. Proc Wind 2003 ASME Wind Energy Symp 2003. https://doi.org/10.1115/WIND2003-865.
[26] Saranyasoontorn K, Manuel L. Design loads for wind turbines using the environmental contour method. J Sol Energy Eng 2006;125:554–61. https://doi.org/10.1115/1.2346700.
[27] Hannesdóttir Á, Kelly M, Dimitrov N. Extreme wind fluctuations: joint statistics,

extreme turbulence, and impact on wind turbine loads. Wind Energy Sci 2019;4:325–42. https://doi.org/10.5194/wes-4-325-2019.
[28] Xu Y, Øiseth O, Naess A, Moan T. Prediction of long-term extreme load effects due to wind for cable-supported bridges using time-domain simulations. Eng Struct 2017;148:239–53. https://doi.org/10.1016/J.ENGSTRUCT.2017.06.051.
[29] Xu Y, Øiseth O, Moan T, Naess A. Prediction of long-term extreme load effects due to wave and wind actions for cable-supported bridges with floating pylons. Eng Struct 2018;172:321–33. https://doi.org/10.1016/J.ENGSTRUCT.2018.06.023.
[30] Davenport AG. The relationship of reliability to wind loading. J Wind Eng Ind Aerodyn 1983;13:3–27. https://doi.org/10.1016/0167-6105(83)90125-3.
[31] Kareem A. Aerodynamic response of structures with parametric uncertainties. Struct Saf 1988;5:205–25. https://doi.org/10.1016/0167-4730(88)90010-0.
[32] Solari G. Wind-excited response of structures with uncertain parameters. Probabilistic Eng Mech 1997;12:75–87. https://doi.org/10.1016/S0266-8920(96)00027-6.
[33] Zhang L, Li J, Peng Y. Dynamic response and reliability analysis of tall buildings subject to wind loading. J Wind Eng Ind Aerodyn 2008;96:25–40. https://doi.org/10.1016/J.JWEIA.2007.03.001.
[34] Pagnini LC, Solari G. Gust buffeting and turbulence uncertainties. J Wind Eng Ind Aerodyn 2002;90:441–59. https://doi.org/10.1016/S0167-6105(01)00202-1.
[35] Pagnini L. Reliability analysis of wind-excited structures. J Wind Eng Ind Aerodyn 2010;98:1–9. https://doi.org/10.1016/J.JWEIA.2009.08.010.
[36] Seo D, Caracoglia L. Statistical buffeting response of flexible bridges influenced by errors in aeroelastic loading estimation. J Wind Eng Ind Aerodyn Wind Eng Ind Aerodyn 2012;104–106:129–40. https://doi.org/10.1016/j.jweia.2012.03.036.
[37] Seo D, Caracoglia L. Estimating life-cycle monetary losses due to wind hazards: Fragility analysis of long-span bridges. Eng Struct 2013;56:1593–606. https://doi.org/10.1016/j.engstruct.2013.07.031.
[38] Solari G, Piccardo G. Probabilistic 3-D turbulence modeling for gust buffeting of structures. Probabilistic Eng Mech 2001;16:73–86. https://doi.org/10.1016/S0266-8920(00)00010-2.
[39] Moan T, Gao Z, Ayala-Uraga E. Uncertainty of wave-induced response of marine structures due to long-term variation of extratropical wave conditions. Mar Struct 2005;18:359–82. https://doi.org/10.1016/J.MARSTRUC.2005.11.001.
[40] Jonathan P, Flynn J, Ewans K. Joint modelling of wave spectral parameters for extreme sea states. Ocean Eng 2010;37:1070–80. https://doi.org/10.1016/J.OCEANENG.2010.04.004.
[41] Ewans K, Jonathan P. Evaluating environmental joint extremes for the offshore industry using the conditional extremes model. J Mar Syst 2014;130:124–30. https://doi.org/10.1016/J.JMARSYS.2013.03.007.
[42] Salvadori G, Tomasicchio GR, D'Alessandro F. Practical guidelines for multivariate analysis and design in coastal and off-shore engineering. Coast Eng 2014;88:1–14. https://doi.org/10.1016/J.COASTALENG.2014.01.011.
[43] Montes-Iturrizaga R, Heredia-Zavoni E. Environmental contours using copulas. Appl Ocean Res 2015;52:125–39. https://doi.org/10.1016/J.APOR.2015.05.007.
[44] Eckert-Gallup AC, Sallaberry CJ, Dallman AR, Neary VS. Application of principal component analysis (PCA) and improved joint probability distributions to the inverse first-order reliability method (I-FORM) for predicting extreme sea states. Ocean Eng 2016;112:307–19. https://doi.org/10.1016/J.OCEANENG.2015.12.018.
[45] Haver S. Wave climate off northern Norway. Appl Ocean Res 1985;7:85–92. https://doi.org/10.1016/0141-1187(85)90038-0.
[46] Gumbel EJ. Statistics of extremes. New York: Columbia University Press; 1958.
[47] Madsen HO, Krenk S, Lind NC. Methods of structural safety. New York: Dover Publications; 1986.
[48] Rosenblatt M. Remarks on a Multivariate Transformation. Ann Math Stat 1952;23:470–2.
[49] Kaimal J, Wyngaard J, Izumi Y, Coté OR. Spectral characteristics of surface-layer turbulence. Q J R Meteorol Soc 1972;98. https://doi.org/10.1002/qj.49709841707.
[50] Davenport AG. The spectrum of horizontal gustiness near the ground in high winds. Q J R Meteorol Soc 1961;87:194–211. https://doi.org/10.1002/qj.49708737208.
[51] Statens-Vegvesen. The Hardanger Bridge: Design basis - Wind characteristics. Norway: 2006.
[52] Lieblein J. Efficient methods of extreme-value methodology. Washington D.C.: 1974.
[53] Cook NJ. Towards better estimation of extreme winds. J Wind Eng Ind Aerodyn 1982;9:295–323.
[54] Harris RI. Improvements to the 'Method of Independent Storms'. J Wind Eng Ind Aerodyn 1999;80:1–30. https://doi.org/10.1016/S0167-6105(98)00123-8.
[55] Jain A, Jones NP, Scanlan RH. Coupled aeroelastic and aerodynamic response analysis of long-span bridges. J Wind Eng Ind Aerodyn 1996;60:69–80. https://doi.org/10.1016/0167-6105(96)00024-4.
[56] Jain A, Jones NP, Scanlan RH. Coupled flutter and buffeting analysis. J Struct Eng 1996;122:716–25. https://doi.org/10.1061/(ASCE)0733-9445(1996)122:7(716).
[57] Chen X, Kareem A, Matsumoto M. Multimode coupled flutter and buffeting analysis of long span bridges. J Wind Eng Ind Aerodyn 2001;89:649–64. https://doi.org/10.1016/S0167-6105(01)00064-2.
[58] Øiseth O, Rönnquist A, Sigbjörnsson R. Simplified prediction of wind-induced response and stability limit of slender long-span suspension bridges, based on modified quasi-steady theory: A case study. J Wind Eng Ind Aerodyn 2010;98:730–41. https://doi.org/10.1016/j.jweia.2010.06.009.
[59] Katsuchi H, Jones NP, Scanlan RH, Akiyama H. Multi-mode flutter and buffeting analysis of the Akashi-Kaikyo bridge 1998;77–78:431–41. http://doi.org/10.1016/S0167-6105(98)00162-7.
[60] Python Software Foundation. Python Language Reference; 2019.
[61] Dassault Systèmes W. ABAQUS;2018.
[62] Siedziako B, Øiseth O, Rønnquist A. An enhanced forced vibration rig for wind tunnel testing of bridge deck section models in arbitrary motion. J Wind Eng Ind Aerodyn 2017;164:152–63. https://doi.org/10.1016/J.JWEIA.2017.02.011.
[63] Larose GL. The dynamic action of gusty winds on long-span bridges: The dynamic action of gusty winds on long-span bridges; 1997.
[64] Standard Norge. Eurocode 1: Actions on structures - Part 1-4: General actions, Wind actions; 2009.
[65] Scanlan RH, Tomko JJ. Airfoil and bridge deck flutter derivatives. J Eng Mech Div 1971;97:1717–37.
[66] Zasso A. Flutter derivatives: Advantages of a new representation convention. J Wind Eng Ind Aerodyn 1996;60:35–47. https://doi.org/10.1016/0167-6105(96)00022-0.
[67] The SciPy Community. SciPy.org. May 17 2019. https://docs.scipy.org/doc/scipy/reference/generated/scipy.optimize.minimize.html [accessed August 22, 2019].